



JOHANNES KEPLER
UNIVERSITÄT LINZ
Netzwerk für Forschung, Lehre und Praxis

Electroabsorption in Organic Diodes

Diplomarbeit zur Erlangung des akademischen Grades eines
Diplom Ingenieurs

in der Studienrichtung
Wirtschaftsingenieurwesen - Technische Chemie

eingereicht von
Christoph Lungenschmied

angefertigt am
Linz Institute for Organic Solar Cells (LIOS)

unter der Betreuung von
o.univ. Prof. Dr. Serdar N. Sariciftci

Linz, Juni 2004

Elektroabsorption in Organischen Dioden

Zusammenfassung

Das in organischen Halbleiterbauelementen herrschende elektrische Feld ist ein entscheidender Faktor für deren Leistungsfähigkeit. Es ist die treibende Kraft für Effekte wie die Ladungsträgermobilität oder auch die Größe des Injektionsstroms.

Ein von außen an diese Bauelemente angelegtes elektrisches Feld bewirkt eine Änderung der Absorption, die mit Hilfe optischer Methoden gemessen werden kann.

Ziel dieser Arbeit ist es, das elektrische Feld in modernen organischen Halbleiterbauelementen wie Polymerleuchtdioden oder organischen Solarzellen zu bestimmen. Für die Leuchtdioden werden Derivate der konjugierten Polymere Polyphenylenvinyl (PPV) und Polythiophen verwendet und der Einfluss verschiedener Schichten an den Grenzflächen zwischen Polymer und Elektroden untersucht. Diese zusätzlichen Schichten werden verwendet, um die Ladungsträgerinjektion in das Polymer zu verbessern.

Des Weiteren wird auch das elektrische Feld in Dioden mit einer aktiven Schicht aus einem löslichen C_{60} Fullerenderivat bestimmt.

Abschließend werden Solarzellen aus Mischungen dieser Komponenten, Polymer als Elektronendonator und Fulleren als Akzeptor untersucht.

Electroabsorption in Organic Diodes

Abstract

The electric field across the active layer is an important parameter for several essential processes in organic semiconductor devices. It is the driving force for effects such as charge carrier mobility and current injection. Electroabsorption (EA) is a method to directly and noninvasively probe the electric field inside the device. By applying an external electric field the absorption is shifted. These changes can be optically detected.

The aim of this work is to study the electric field present in the active layer of state of the art organic semiconductor devices. Polymer light emitting diodes (PLEDs) and bulk heterojunction photovoltaic devices are subject of this study. For the PLED structures employing a layer of a poly-phenylene vinylene (PPV) or a polythiophene derivative the influence of various interfacial layers is examined. These interfacial layers were applied between the electrodes and the polymer layer, both of them promoting charge carrier injection. Furthermore, the electric field in diodes made from a soluble C_{60} fullerene derivative was studied. Finally electroabsorption is measured on bulk heterojunction photovoltaic devices incorporating both groups of the previously studied materials: the conjugated polymer as donor and the fullerene as acceptor component.

Contents

1	Introduction	1
1.1	Motivation	1
1.2	Electric-Field Modulation Spectroscopy	2
1.3	How does Electroabsorption work?	3
1.3.1	The Stark Effect	3
1.3.2	Dependence on the Electric Field	4
1.3.3	Spectral Line Shape	6
2	Experimental	8
2.1	The Experimental Apparatus	8
2.2	Device Preparation	11
2.2.1	Substrate Preparation	11
2.2.2	Materials	11
2.2.3	Evaporation of the Top Electrodes	14
2.2.4	Installation	15
3	Results and Discussion	16
3.1	MDMO-PPV Devices	17
3.1.1	Spectra of MDMO-PPV	17
3.1.2	ITO - MDMO-PPV - Al Devices	23
3.1.3	ITO - MDMO-PPV - LiF - Al Devices	25
3.1.4	ITO - PEDOT - MDMO-PPV - Al Devices	27
3.1.5	ITO - PEDOT - MDMO-PPV - LiF - Al Devices	28
3.1.6	Summary of the Results	29
3.2	P3HT Devices	33
3.2.1	ITO - P3HT - Al Devices	33
3.2.2	ITO - P3HT - LiF - Al Devices	43
3.2.3	ITO - PEDOT - P3HT - Al Devices	45
3.2.4	ITO - PEDOT - P3HT - LiF - Al Devices	49
3.2.5	Summary of the Results	51
3.3	PCBM Devices	55
3.4	MDMO-PPV/PCBM Blends	60
3.4.1	MDMO-PPV/PCBM Blends from Chlorobenzene	60

3.4.2	MDMO-PPV/PCBM Blends from Toluene	65
3.5	P3HT/PCBM Blends	73
3.5.1	Untreated Devices Employing P3HT/PCBM Blends as Active Layer	73
3.5.2	P3HT/PCBM Blends after Postproduction Treatment	76
4	Conclusion	83

Acknowledgement

First and foremost I want to thank my parents for their support during the years of my studies.

I would also like to thank my supervisor Prof. Dr. N.S. Sariciftci, who made this work possible as well as Dr. Markus Scharber, DI Christoph Winder and Dr. Helmut Neugebauer for their kind advice.

Furthermore DI Attila Mozer and DI Gebhard Matt for helping me to overcome many problems in the laboratory and of course thanks to all other members of LIOS in the last year, Andrej Andreev, Assefa Sergawie Asemahegne, Elif Arici, Luis Campos, Antonio Cravino, Gilles Dennler, Martin Drees, Martin Egginger, Anita Fuchsbauer, Serap Günes, Alexander Gusenbauer, Sandra Hofer, Harald Hoppe, Robert Köppe, Nenad Marjanovic, Farideh Meghdadi, Dieter Meissner, Birendra Singh, Daniela Stoenescu and Manfred Lipp, Birgit Paulik, Petra Neumair and Elke Bradt as well as the staff of Konarka Austria Patrick Denk, Markus Koppe, David Mühlbacher, Franz Padinger, Roman Rittberger and Christoph Topf.

Thank you for the good time

Chapter 1

Introduction

1.1 Motivation

When H. Shirakawa, A.G. MacDiarmid and A.J. Heeger discovered electric conductivity in polyacetylene in 1977, the interest of the scientific world was drawn to a new group of materials with promising properties [1, 2, 3]. Since then many of these conducting polymers have been synthesized to be used in a whole range of different applications.

Much effort has been invested in science and technology of these materials resulting in already commercially available products and several applications being on the verge of entering the market.

Reflecting the successful development H. Shirakawa, A.G. MacDiarmid and A.J. Heeger were awarded the Nobel Prize for Chemistry in 2000.

Especially in polymer light-emitting diodes (PLEDs) and organic photovoltaic devices a crucial parameter for efficient operation is the electric field present in the device's active layer.

The two important processes, current injection into PLEDs at the organic/electrode interface [4] and charge carrier mobility in the polymer are field dependent [5]. Therefore the internal electric field distribution in PLEDs under operation is a critical parameter from theoretical and applications perspectives [6, 7, 8]. In organic photovoltaic devices the electric field is the driving force to extract the created charge carriers and therefore of paramount importance for the efficiency.

Electromodulation spectroscopy (EM) [5, 9, 10] offers a noninvasive method to optically probe these internal electric fields inside the devices.

While EM spectra contain contributions originating from various effects of the applied electric field, the term electroabsorption (EA) relates to the Stark effect.

Making use of this effect allows to determine the electric field present in polymer layers or even ready-made devices.

1.2 Electric-Field Modulation Spectroscopy

An externally applied electric field influences the interaction of a molecule with light even if this field is much smaller than those present inside the atoms and molecules.

Electric-field modulation spectroscopy measures these changes with respect to the applied field. The interpretation of its spectral response significantly adds information to absorption or reflectance spectra [11].

If the observed quantity is the change of absorption features, the term electroabsorption is used for this method.

Initially applied to crystalline inorganic semiconductors, early work was done on interpreting and predicting electroreflectance (ER) spectra [12, 13]. The knowledge obtained in the work on inorganic crystals soon was used to apply the method to newly synthesized organic semiconductors like polyacetylene [14].

In the group of G. Weiser pioneering work was done interpreting the spectra obtained from electric-field modulation spectroscopy on conjugated polymers. First, the focus was on single crystalline polydiacetylene [15] showing the most similarities with inorganic semiconductors, but later EA was used to study disorder effects in polydiacetylene substituted with side groups [16]. The EA experiments revealed a pronounced anisotropy: Due to the higher polarizability of the conjugated segments along the polymer's backbone, applying the external electric field parallel to the polymer chains resulted in a higher response than perpendicular to the π -electron system. To achieve the higher signal, the electrodes were evaporated as interdigitated structures on top of the polymer.

A different approach was chosen by the group around I.H. Campbell and D.L. Smith. Instead of measuring in transmission geometry, they built up a setup to measure metal/polymer/metal sandwich structures in reflection geometry [17], which is described more closely in section 2.1. This method enabled them to observe a built-in potential across the polymer layer when different metals were used as anode and cathode materials [17, 18].

They aimed to find the maximum electric field created by the difference in the electrodes' work functions that can be supported by a given organic material.

Measuring the built-in field was established as a technique to determine material properties of semiconducting polymers.

As research activities on polymer light-emitting diodes increased, EA measurements were done on LED structures employing transparent indium tin oxide (ITO) instead of metal anodes. This step from pure material characterization to determination of device properties was taken by the group of R.H. Friend. They determined the influence of a layer of poly(3,4-

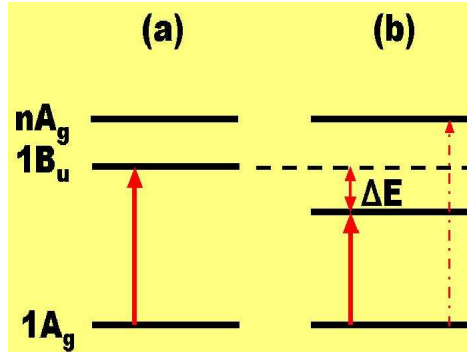


Figure 1.1: Energy levels affected by the Stark effect; (a) field free case, (b) split energy levels due to an electric field.

ethylenedioxythiophene) doped with poly(styrenesulfonate) (PEDOT:PSS) on the internal electric field of PLED devices [19]. Also thickness dependent studies on the influence of LiF as cathodic interfacial layer on the built-in potential have been carried out [20], but led to results contradicting a second publication on this topic by Yoon et al. [21].

The aim of this work is to systematically study the internal electric field by means of EA in two different conducting polymers and a C_{60} -derivative to find the influence of the different layers used in efficient state of the art organic LEDs and photovoltaic devices.

1.3 How does Electroabsorption work?

1.3.1 The Stark Effect

Even if there are no permanent dipoles present in the material, it will interact with an applied electric field. Depending on its polarizability dipoles will be induced.

A dipole moment can only have two stationary positions in a homogeneous electric field: in direction of the field or opposite. Therefore every energy level prior to applying the field will be split in two energy levels symmetric around the field-free level.

The level lower in energy represents the position opposite to the electric field and the high energy level the position in direction of the field.

The Stark effect describes the splitting of the energy levels in the presence of an electric field. Fig. 1.1 illustrates two effects resulting from this splitting: The more important one is the red shift of the $1A_g \rightarrow 1B_u$ transition, the so-called excitonic Stark shift (ΔE), but the applied electric field can also couple the $1A_g$ level to a higher lying state of even parity. This usually forbidden transition between even parity states becomes allowed in the

presence of an electric field (dot and dash line in Fig. 1.1) [11]. In the following, E will represent the photon energy, E_l the electric field of the light beam and F an externally applied electric field.

The excitonic Stark shift is described as follows:

$$\Delta E = \vec{\mu} \cdot F + \frac{1}{2} \cdot \Delta\vec{p} \cdot F^2 \quad (1.1)$$

Equation (1.1) consists of two parts, the first scaling linearly and the second quadratically with the electric field. While the linear part prevails in the presence of permanent dipoles ($\vec{\mu}$ being the permanent dipole moment), the quadratic part describes the interaction of induced dipoles with an external electric field. $\Delta\vec{p}$ is a second order tensor and represents the polarizability of the medium.

1.3.2 Dependence on the Electric Field

The interaction of the electron shells of the atoms with the modulated electric field of an incident light beam leads to a displacement current. The resulting polarization is proportional to the electric field of the light as long as the light intensity is sufficiently small.

Equation (1.2) describes the connection between the dipole moment per unit volume (the polarization \vec{P}) and the polarizing electric field of the light beam \vec{E}_l .

$$\vec{P} = \varepsilon_0 \cdot \chi \cdot \vec{E}_l \quad (1.2)$$

ε_0 is the dielectric constant of the vacuum, while the susceptibility χ represents the macroscopic polarizability of the medium.

A nonlinearity of the response to the light can be introduced by very high illumination or by an externally applied electric field, inducing dipoles in the medium.

An applied electric field (field strength F) causes a nonlinearity described by a field dependent susceptibility χ :

$$\chi = \chi^{(1)} + \chi^{(2)} \cdot F + \chi^{(3)} \cdot F^2 + \dots \quad (1.3)$$

For molecules with inversion symmetry like conjugated polymers and fullerenes, all even terms of χ vanish. Changing the direction of the electric field changes only the sign, not the absolute value of the polarization. Therefore both equations

$$P_2 = \varepsilon_0 \cdot \chi^{(2)}(+E_l)^2 \quad \text{and} \quad -P_2 = \varepsilon_0 \cdot \chi^{(2)}(-E_l)^2$$

have to hold true, which is only possible if $P_2 = \chi^{(2)} = 0$. $\chi^{(3)}$ remains as the lowest order nonlinear susceptibility [22].

For many molecules a three-level model presented in Fig. 1.1 consisting of the ground state $1A_g$, the first allowed $1B_u$ and a nA_g was found to account for $\chi^{(3)}$ spectra [23]. EA is a third-order non linear susceptibility phenomenon depending on the square of the applied electric field and linearly on the photon energy [12]. To make use of this finding, a connection between the induced $\chi^{(3)}$ and the measured change in the transmitted light intensity $\frac{\Delta I}{I}$ has to be found.

The connection between the susceptibility χ and the dielectric function ε is given by:

$$\varepsilon = 1 + \chi \quad (1.4)$$

The Maxwell relation correlates the dielectric function ε with the complex refractive index $\tilde{n} = n + i\kappa$:

$$\varepsilon = \varepsilon_1 + i\varepsilon_2 = (n + i\kappa)^2 \quad (1.5)$$

From equation (1.5) for the real part of the dielectric function (ε_1)

$$\varepsilon_1 = n^2 - \kappa^2 \quad (1.6)$$

is obtained, while the imaginary part (ε_2) is proportional to the absorption constant $\alpha(E)$

$$\varepsilon_2 = 2n\kappa = \frac{nc}{\omega} \alpha(E) \quad (1.7)$$

where c is the speed of light and ω the frequency of the incident light [11]. Equation (1.7) describes the relation between the imaginary part of the dielectric function ε_2 and the absorption coefficient. Due to equation (1.4), the imaginary part of the susceptibility ($Im\chi$) is directly proportional to the absorption constant $\alpha(E)$.

Equation (1.8) describes the relation between the change in transmittance $\frac{\Delta I}{I}$ and the change in the absorption constant ($\Delta\alpha(E)$) for reflection geometry (double path transmission), where d is the layer thickness.

$$\Delta\alpha(E) = -\frac{1}{2d} \cdot \frac{\Delta I}{I} \quad (1.8)$$

Due to the dependence of χ on the applied electric field (equation (1.3)), the proportionality between the observed change in the transmittance $\frac{\Delta I}{I}$ and the actual electric field is given by the photon energy (E) dependent imaginary part of the third-order non linear susceptibility $Im\chi^{(3)}(E)$:

$$\frac{\Delta I}{I} \propto Im\chi^{(3)}(E) \cdot F^2 \quad (1.9)$$

If the electric field F is caused by an externally applied combined DC and AC bias (V) and the presence of an internal electric field inside the film (V_{int})

is assumed, plugging equations (1.10) into equation (1.9) yields equation (1.11).

$$V = V_0 + V_{AC} \cdot \sin(\omega t) \quad \text{with} \quad V_0 = V_{DC} - V_{int} \quad (1.10)$$

$$\frac{\Delta I}{I} \propto \text{Im}\chi^{(3)}(E) \cdot \left(\underbrace{(V_{DC} - V_{int})}_{V_0} + V_{AC} \cdot \sin(\omega t) \right)^2 \quad (1.11)$$

From equation (1.11), equation (1.12) is derived as:

$$\frac{\Delta I}{I} \propto \text{Im}\chi^{(3)}(E) \cdot \left\{ \frac{1}{2} V_{AC}^2 \cdot (1 - \cos(2\omega t)) + 2V_0 \cdot V_{AC} \cdot \sin(\omega t) + V_0^2 \right\} \quad (1.12)$$

Equation (1.12) can be separated into two parts, one dependent on the first harmonic (1ω), the other on the second harmonic (2ω) change in transmittance:

$$\frac{\Delta I}{I}(\omega) \propto (V_{DC} - V_{int}) \cdot V_{AC} \cdot \sin(\omega t) \quad (1.13)$$

$$\frac{\Delta I}{I}(2\omega) \propto V_{AC}^2 \cdot \cos(2\omega t) \quad (1.14)$$

While the first harmonic (1ω) response is proportional to the product of the resulting DC field and AC amplitude, the second harmonic (2ω) signal depends on the square of the AC amplitude.

Equation (1.13) presents a way to determine the internal electric field present in the film: The EA response vanishes, if the term $(V_{DC} - V_{int})$ is zero (Equation (1.13)). This is the case, when the applied DC bias is of the same magnitude, but opposite direction of the internal electric field.

The experimental realization is done by keeping the AC amplitude constant and changing the applied DC bias until the external DC voltage exactly cancels the internal electric field.

1.3.3 Spectral Line Shape

The field induced change of the absorption coefficient $\Delta\alpha(E)$ can be described as the difference between the absorption in the presence of an electric field $\alpha^F(E)$ and the unperturbed absorption $\alpha(E)$:

$$\Delta\alpha(E) = \alpha^F(E) - \alpha(E) \quad (1.15)$$

In equation (1.1), the Stark effect is described as a red shift of the absorption in the presence of an electric field compared to the field free case. Therefore $\alpha^F(E)$ is proportional to the unperturbed absorption at the shifted wavelength:

$$\alpha^F(E) = k\alpha(E + \Delta E) \quad (1.16)$$

Carrying out a Taylor expansion of $\alpha(E + \Delta E)$ up to the second order yields for $\Delta\alpha(E)$ [24]:

$$\Delta\alpha(E) = (k - 1) \cdot \alpha(E) + k \cdot \frac{d\alpha(E)}{dE} \cdot \Delta E + \frac{1}{2} \cdot k \cdot \frac{d^2\alpha(E)}{dE^2} \cdot (\Delta E)^2 \quad (1.17)$$

Equation (1.17) shows terms scaling with the first and the second derivative of the unperturbed absorption coefficient. A first derivative line shape points out a prevailing effect of field induced dipoles, while finding a second derivative line shape is correlated with the presence of permanent dipoles [11].

Chapter 2

Experimental

2.1 The Experimental Apparatus

The homemade electroabsorption setup used for the experiments is operated in so-called reflection geometry. This means that the probe light beam has to pass through the film once, is reflected at the back electrode and passes through the film a second time. Of all the reflections shown in Fig. 2.2, this is the only one to be influenced by the electric field applied between ITO and Al. Fig. 2.1 schematically shows the instruments and the path of the aligned probe light beam.

As light source a 24 V, 250 W tungsten lamp (XENOPHOT HLX 64655) is used, powered by a very stable power supply (SVX 1530/LAX 1530 from Müller GmbH Elektronik-Optik). Before entering the monochromator (Acton Research SP-150, 150 g/mm grating, with an 800 nm blaze) the light beam passes through a filter, cutting off wavelengths below 450 nm.

The entrance and exit slits are opened by 0.3 mm, a good compromise delivering sufficient light intensity with a spectral resolution better than 10 nm. Via a system of three lenses and a mirror for precision alignment, the probe beam is focused onto the active area of the sample inside the cryostat, where it is mounted on a cold finger.

The cryostat (Oxford Instruments Optistat DN-V) can be filled with liquid nitrogen and is connected to a temperature controller. Via a manually adjustable valve, regulating the flow of liquid nitrogen cooling the cold finger and a heating system, any temperature between 77 K and 500 K can be adjusted.

Experiments were only carried out at room temperature or 77 K.

The reflection coming from the Al back electrode is collected by a lens and focused on a Si-detector, delivering a signal proportional to the incoming light intensity to the lock-in amplifier (Stanford Research Systems SRS 830).

A combined DC and AC voltage produced by the function generator (Stanford Research Systems DS345) is applied across the sample, connecting the

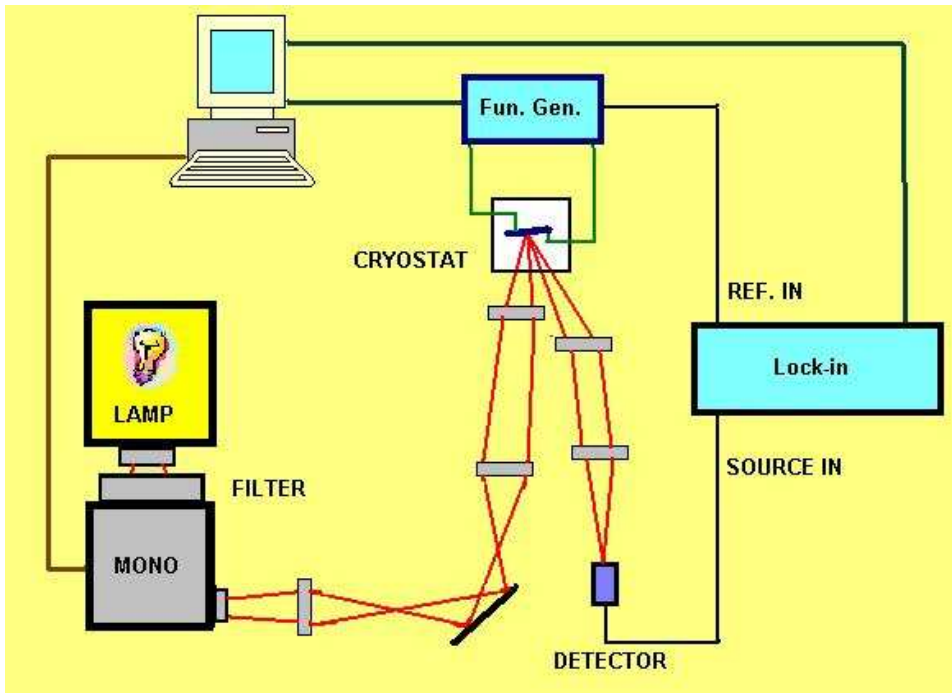


Figure 2.1: Schematic picture of the EA setup used for the experiments.

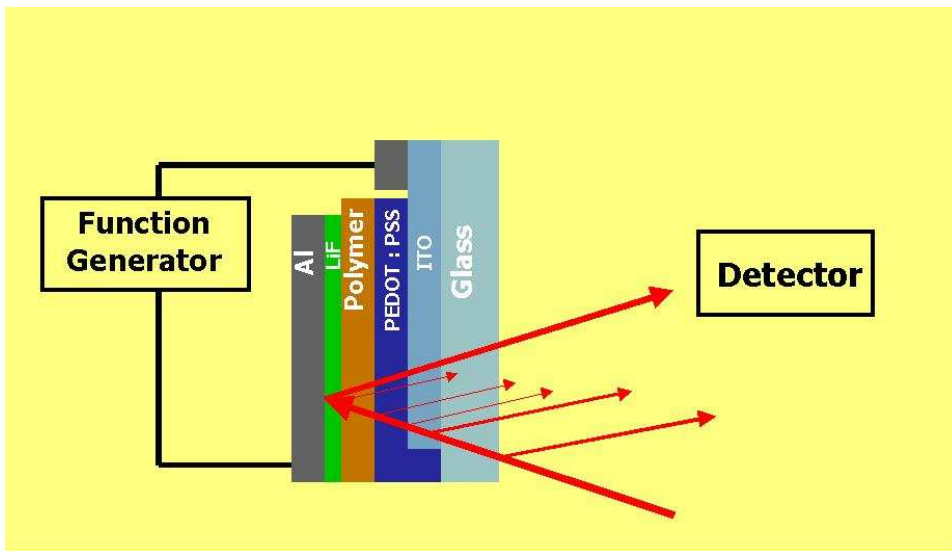


Figure 2.2: Schematic picture of the possible reflections at the interfaces of the device in sandwich geometry.

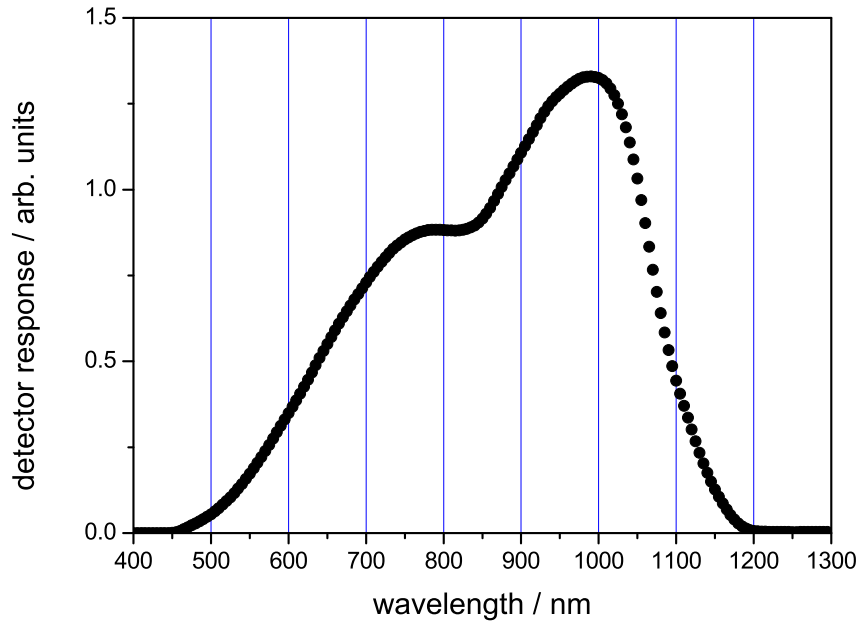


Figure 2.3: Spectral detector response of the reflection on a glass - ITO - Al mirror describing the performance of the EA setup.

+ to the ITO and the - to the Al. A reference signal of the same frequency and phase is delivered to the lock-in amplifier.

From the computer, the monochromator can be set to a certain wavelength, the parameters for the function generator and the lock-in amplifier can be adjusted and the response from the lock-in is recorded. The homemade programs allow operation in two ways: Certain DC and AC values are set and the program records the response of the lock-in while scanning through a predefined wavelength range or AC amplitude and wavelength are constant while the DC offset is changed in steps.

If no voltage is applied and instead a chopper wheel is set up in front of the monochromator's exit slit, the signal coming from the detector is proportional to the double path transmission (DPT) at that wavelength. It can be read out from the lock-in if referenced to the chopping frequency.

For every measured wavelength the EA response is normalized to this signal to get rid of the spectral response due to the characteristics of the setup.

These characteristics include the intensity distribution of the lamp, the performance of the monochromator and the sensitivity of the detector. The performance of the EA setup is presented in Fig. 2.3 by showing the spec-

tral detector response to the reflection at a glass - ITO - Al mirror read out from the lock-in amplifier.

While the EA spectra are normalized to the DPT detector response, the DPT spectra are normalized to the reflection at a glass - ITO - Al mirror. The transmission spectra are recorded with a chopping frequency of 173 Hz, the EA with an AC modulation frequency of 2023 Hz.

Also the current - voltage (I-V) characteristics of the samples installed inside the cryostat can be directly measured by plugging a Keithley 2400 source meter to the connectors on the cryostat. Knowing the active area allows the calculate the current density - voltage (J-V) characteristics.

2.2 Device Preparation

2.2.1 Substrate Preparation

The PLED and photovoltaic devices were prepared in sandwich geometry as schematically shown in Fig. 2.2. Substrates for these devices were 1.5 cm \times 1.5 cm large glass sheets covered with ITO (Merck). To ensure secure connection of the Al cathode without risking the connector tip to punch through the Al layer and shortcut to the ITO, part of the ITO was removed by etching.

This was done by exposing the surface to a strong acid ($HCl_{conc.} : HNO_3_{conc.} : H_2O = 4.6 : 0.4 : 5$) for 20 minutes. The part where ITO should remain was coated with nail varnish to protect it from the acid. The varnish was removed by rinsing with acetone. For thorough cleaning the substrates subsequently underwent two cycles of 20 minutes in acetone and one in 2-propanole in an ultrasonic bath.

After drying, the substrates were covered with PEDOT:PSS or the active layer, depending on the desired device structure.

2.2.2 Materials

PEDOT:PSS

Poly(3,4-ethylenedioxythiophene) doped with poly(styrenesulfonate) (in the following abbreviated as PEDOT:PSS or just PEDOT) was spin coated onto the ITO twice to act as an interfacial hole contact and electron blocking layer in the finished device.

In all the samples prepared for this study, PEDOT:PSS from the same batch (purchased from Bayer AG) was used. The chemical structure is given in Fig. 2.4.

For the spin coating process a program was used, where the sample holder is accelerated with a ramp time of 4 s to 1500 rpm and kept at that rotational speed for 40 s. Subsequently the samples undergo 20 s of rotation with 2000 rpm.

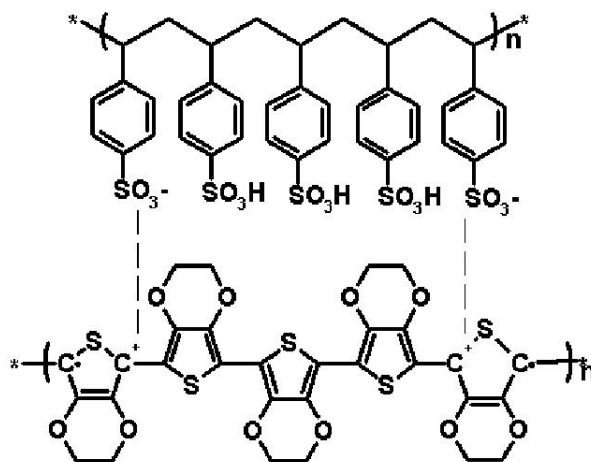


Figure 2.4: Chemical structure of poly(3,4-ethylenedioxythiophene) and poly(styrenesulfonate), PEDOT:PSS

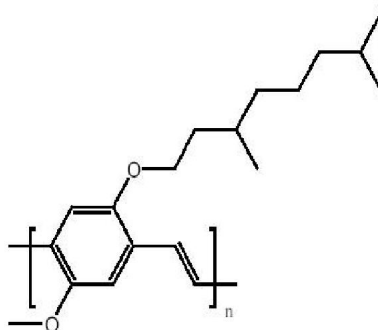


Figure 2.5: Chemical structure of poly[2-methoxy-5-(3',7'-dimethyloctyloxy)-1-4-phenylene vinylene], MDMO-PPV

This standard program is used for all spin casting operations unless explicitly noted.

The coated devices were dried under vacuum over night.

MDMO-PPV

Active layers made from MDMO-PPV, short for poly[2-methoxy-5-(3',7'-dimethyloctyloxy)-1-4-phenylene vinylene] (Fig. 2.5) were spin cast from a 0.5% by weight solution in chlorobenzene. MDMO-PPV is weighed in inside an Ar glove box (MB 204 from Mbraun) and stirred at 50 °C at least for one day prior to spin casting onto the substrates from warm solution.

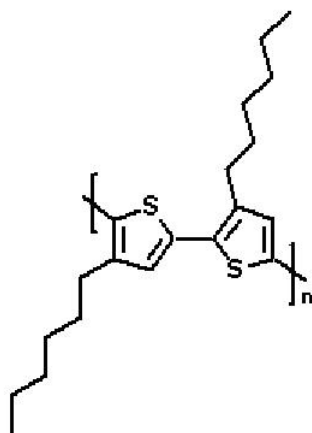


Figure 2.6: Chemical structure of regioregular poly(3-hexylthiophene-2,5-diyl), P3HT

Regioregular P3HT

Thin films (≈ 80 nm) of regioregular P3HT (poly(3-hexylthiophene-2,5-diyl)) were prepared in the same way as those from MDMO-PPV by spin coating from a warm 2% by weight solution in chlorobenzene.

Thicker films employed in the studied ITO - P3HT - Al structures were prepared from a solution in chloroform using doctor blade technique. These were the only devices not prepared by spin coating.

PCBM

To apply PCBM (1-(3-methoxycarbonyl)propyl-1-phenyl [6,6]C₆₀) (Fig. 2.7) layers onto PEDOT coated ITO on glass substrates, the 3% by weight PCBM solution in chlorobenzene was spun inside the glove box using a modified spin cast programme with slower rotation speed in order to achieve increased layer thicknesses. The rotation frequency was decreased by 500 rpm to 1000 rpm for the first 40 s after the ramp time and 1500 rpm for the last 20 s.

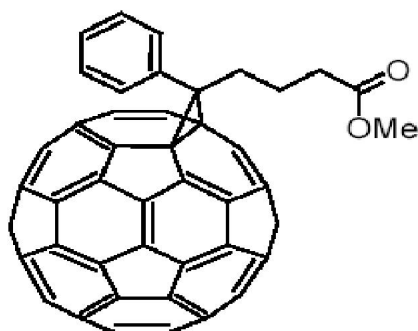


Figure 2.7: Chemical structure of (1-(3-methoxycarbonyl)propyl-1-phenyl [6,6]C₆₁), PCBM

MDMO-PPV/PCBM Blends

MDMO-PPV/PCBM (1:4) blends were prepared with two different solvents: chlorobenzene and toluene.

Besides the difference in the solvent, the preparation was done equally. 1 ml of the solvent was added to 3.5 mg MDMO-PPV and 14 mg PCBM, then the mixture was stirred for two days at approximately 50 °C.

The films were prepared by spin casting.

P3HT/PCBM Blends

The devices studied without postproduction treatment were prepared from blends of the P3HT/PCBM ratio 1:2 (0.5% P3HT and 1% PCBM) in chloroform.

The films that underwent postproduction treatment prior to the EA studies were made from a P3HT/PCBM 2:3 (1.2% P3HT, 1.8% PCBM) solution in chloroform.

The parameters for the postproduction treatment [25], a combined heat and voltage treatment were: 2.7 V, 140 °C for 240 s.

2.2.3 Evaporation of the Top Electrodes

The top electrodes were applied by thermal deposition through a shadow mask at a pressure of approximately 10^{-5} mbar. Tungsten boats were used as source.

Depending on the desired structure the electrode was prepared by one-layer (Al) or two-layer (LiF - Al) deposition.

At least 100 nm thick Al films were deposited to ensure good reflection and some protection of the film against moisture and oxygen.

LiF was applied by evaporating 0.6 nm of the salt directly onto the organic film, afterwards covered by the Al. Thin interfacial layers of LiF are known

to improve electron injection from the Al into the active layer. About the reason for this no consensus has been reached to-date. Some of the proposed mechanisms are listed in reference [26].

2.2.4 Installation

The devices were installed into the cryostat as shown schematically in Fig. 2.2. A small drop of silver paste was put on top of the Al contacts where the connector tips were applied.

Because this installation process was done on air the samples were exposed to oxygen for about 1 minute. After the sample was mounted and contacted, the cryostat was evacuated to pressures better than 10^{-6} mbar. The devices employing P3HT/PCBM active layers were the only exception. To mount them on the sample holder, the cryostat was transferred into the glove box.

Chapter 3

Results and Discussion

In this chapter the results of the EA, J-V characteristic and double path transmission measurements are presented.

The outline of the chapter is chosen to follow the systematic study on the interaction of materials used in state of the art organic semiconductor devices with externally applied electric fields.

The studies on the conducting polymers MDMO-PPV and regioregular P3HT cover the first part. Here the main task is to determine the influence of temperature effects and of interfacial layers like PEDOT:PSS or LiF on the internal electric field present between the electrodes ITO and Al.

Next, diodes using a layer of pristine PCBM are examined. Experiments are only done with devices of the structure ITO - PEDOT - PCBM -LiF - Al to learn about the EA features and the internal electric field of this electron acceptor material.

After the donor and acceptor materials have been studied separately, the third part deals with bulk heterojunction solar cell devices made from polymer/PCBM blends.

For the combination MDMO-PPV/PCBM, films were prepared from different solvents. The EA experiments aim to reveal differences between films spin cast from toluene or chlorobenzene and therefore the influence of the film morphology.

Photovoltaic (PV) devices from P3HT/PCBM blends are investigated to find the influence of the postproduction treatment [25] on the internal electric field and EA spectra.

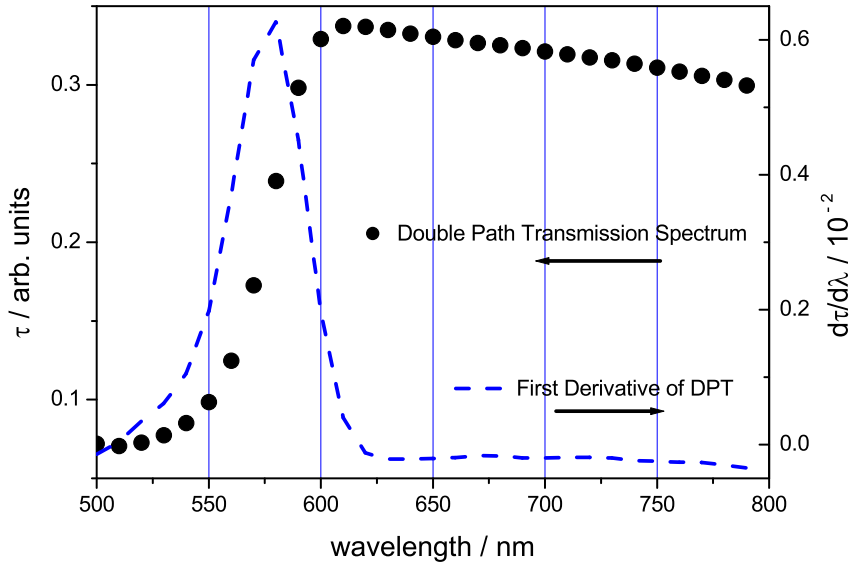


Figure 3.1: Double path transmission (DPT) spectrum of an ITO - MDMO-PPV - Al device and its first derivative, measured at room temperature.

3.1 MDMO-PPV Devices

3.1.1 Spectra of MDMO-PPV

Fig. 3.1 and Fig. 3.2 show the double path transmission (DPT) spectra of an approximately 100 nm thick spin cast MDMO-PPV film on ITO coated glass substrates. An opaque layer of Al acts as reflecting back electrode. When cooling down from room temperature to 77 K, a slight red shift of the spectrum is observed (Fig. 3.2). For both spectra, the first derivative is calculated and included in the figures.

The electroabsorption spectrum obtained at the fundamental frequency of the AC modulation (1ω EA) exhibits the same line shape as the first derivative of the double path transmission spectrum. This is shown for room temperature in Fig. 3.3, for low temperature in Fig. 3.4 and indicates the observation of excitonic Stark shift (see section 1.3.3). As long as the sample is reverse-biased, the peak at 580 nm predicted by the first derivative of the double path transmission spectrum remains the only one in the spectrum. If the modulation of the applied voltage is around 0.5 V in forward direction, an additional peak at 630 nm is observed in the results of the room temperature experiment.

Introducing an interfacial layer of PEDOT:PSS at the anode and LiF at the cathode the EA spectrum at room temperature changes for all applied

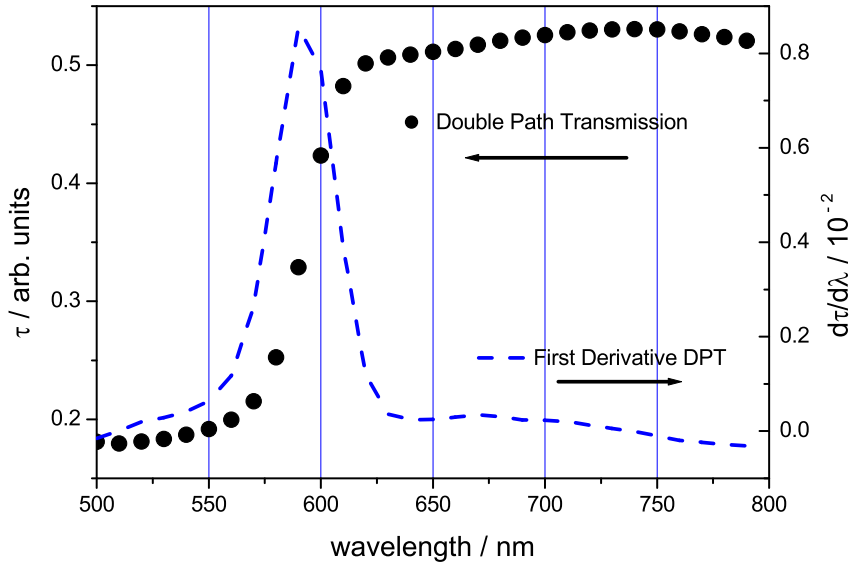


Figure 3.2: Double path transmission (DPT) spectrum and its first derivative of an ITO - MDMO-PPV - Al device measured at 77 K.

DC offsets (Fig. 3.5), while the low temperature spectrum stays unaffected (Fig. 3.6).

The only impact of going from negative to positive DC offsets at 77 K is, that the peak height is reduced.

On the other hand in the room temperature experiment (Fig. 3.5) a new peak is observed to arise adjacent to the initial one at 580 nm. Shifting the DC offset from -2 V to 0 V, the first peak at 580 nm is lowered but still present. This supports the presence of an electric field inside the device. The second peak around 630 nm is increased.

While in the room temperature 1ω EA spectrum of the ITO - MDMO-PPV - Al structure the peak at 630 nm only shows up if a positive DC offset is applied, for the ITO -PEDOT - MDMO-PPV - LiF - Al device two peaks are present in the spectrum even when reverse-biased.

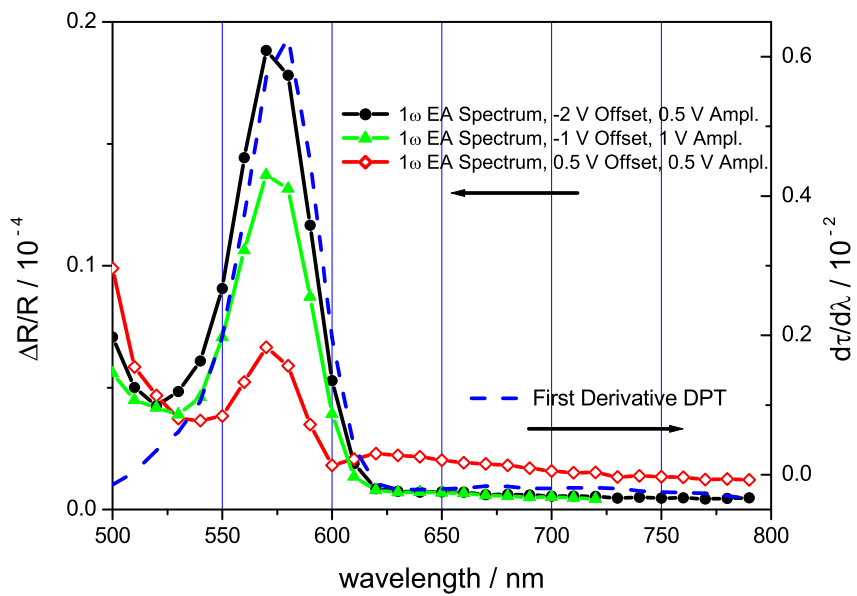


Figure 3.3: First harmonic (1ω) EA spectrum of an ITO - MDMO-PPV - Al device, compared with the first derivative of the double path transmission (DPT) spectrum measured at room temperature; -2 V offset, 0.5 V amplitude (circles); -1 V offset, 1 V amplitude (triangles); 0.5 V offset, 0.5 V amplitude (diamonds).

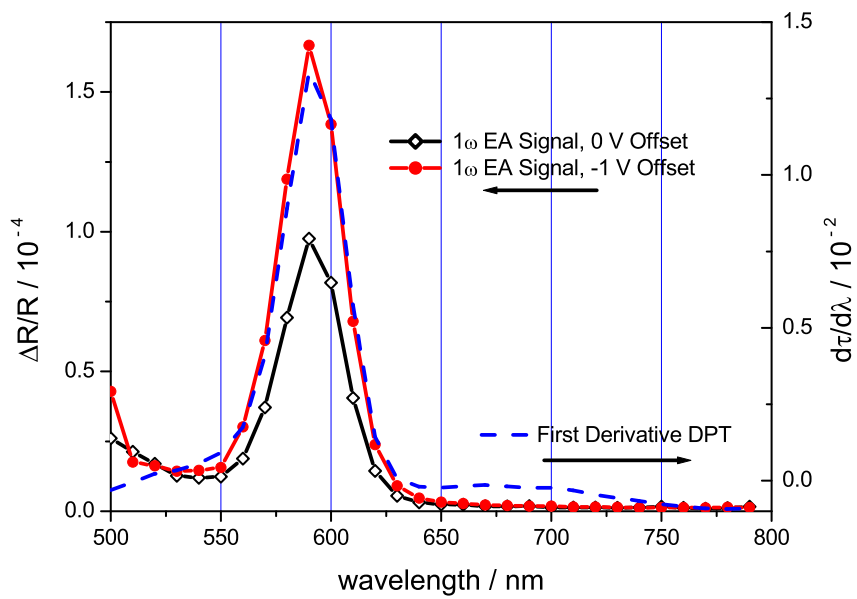


Figure 3.4: 1ω EA spectrum of an ITO - MDMO-PPV - Al device, compared with the first derivative of the double path transmission (DPT) spectrum measured at 77 K; -1 V offset, 1 V amplitude (circles) and 0 V offset, 1 V amplitude (diamonds).

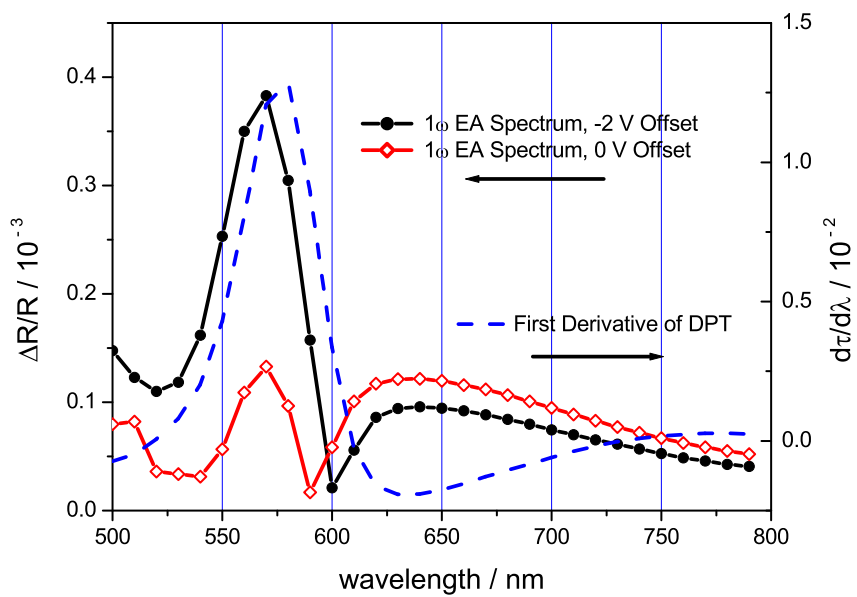


Figure 3.5: 1ω EA spectrum of an ITO - PEDOT - MDMO-PPV - LiF - Al device, compared with the first derivative of the double path transmission (DPT) spectrum measured at room temperature; -2 V offset, 1 V amplitude (circles); 0 V offset, 1 V amplitude (diamonds).

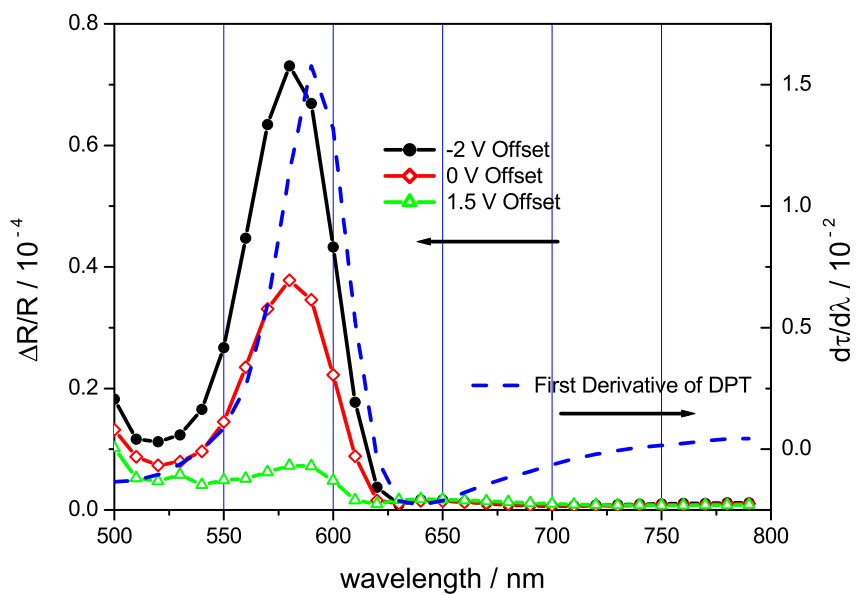


Figure 3.6: 1ω EA spectrum of an ITO - PEDOT - MDMO-PPV - LiF - Al device, compared with the first derivative of the double path transmission (DPT) spectrum measured at 77 K; -2 V offset, 1 V amplitude (filled circles); 0 V offset, 1 V amplitude (diamonds); 1.5 V offset, 1 V amplitude (triangles).

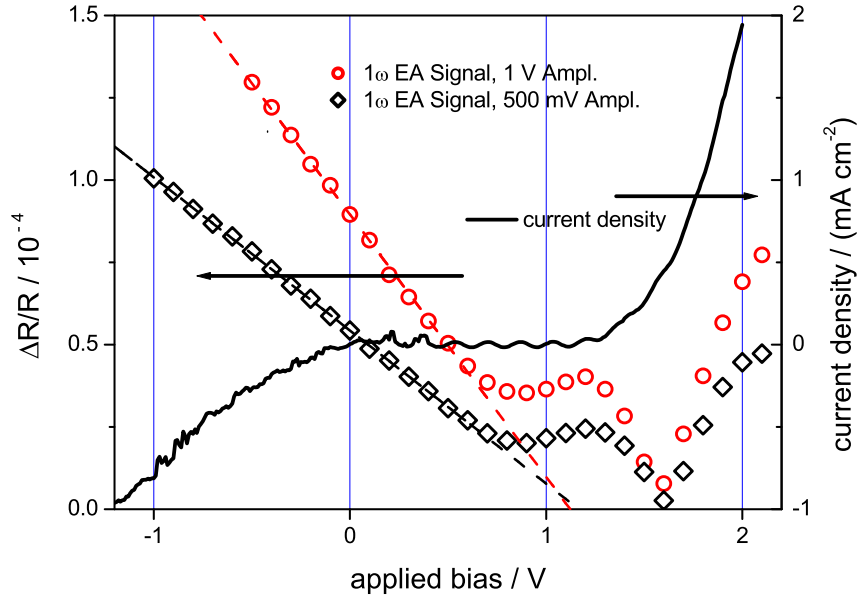


Figure 3.7: Internal electric field measurement and J-V curve measured at room temperature of an ITO - MDMO-PPV - Al device probed at 590 nm; 1 V amplitude (circles) and 500 mV amplitude (diamonds).

3.1.2 ITO - MDMO-PPV - Al Devices

The internal electric field present in the device is measured as described in section 1.3.2: The AC component of the externally applied field is kept constant, while the DC offset is changed in steps.

As can be seen from Fig. 3.7, the response to the applied electric field shows two minima located at 0.9 V and 1.6 V. Just as predicted in equation (1.13) the EA response using an AC amplitude of 1 V (circles) is roughly twice as high as at 500 mV (diamonds). The falling branches can be fitted linearly and the resulting straight lines both intersect the zero line at approximately 1.1 V.

Cooling down the sample with liquid nitrogen and repeating the experiment leads to a much clearer result. Even the rising branch can be determined and fitted linearly. As Fig. 3.8 shows, the point of intersection of the fitted curves with the zero line is located at 1.6 V, where the EA response equals zero and the phase of the lock-in signal changes by 180 degrees, indicating the change of the direction of the electric field responsible for the ES response. Applying 1.6 V, the internal electric field is nulled and therefore no Stark effect can be measured.

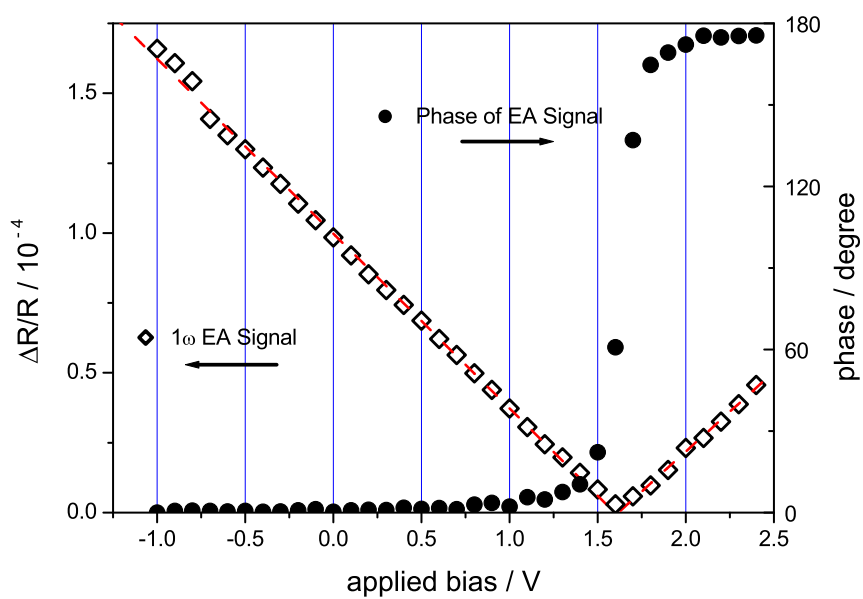


Figure 3.8: Internal electric field measurement and the phase of the 1ω EA signal at 77 K of an ITO - MDMO-PPV - Al device probed at 590 nm; 1 V amplitude.

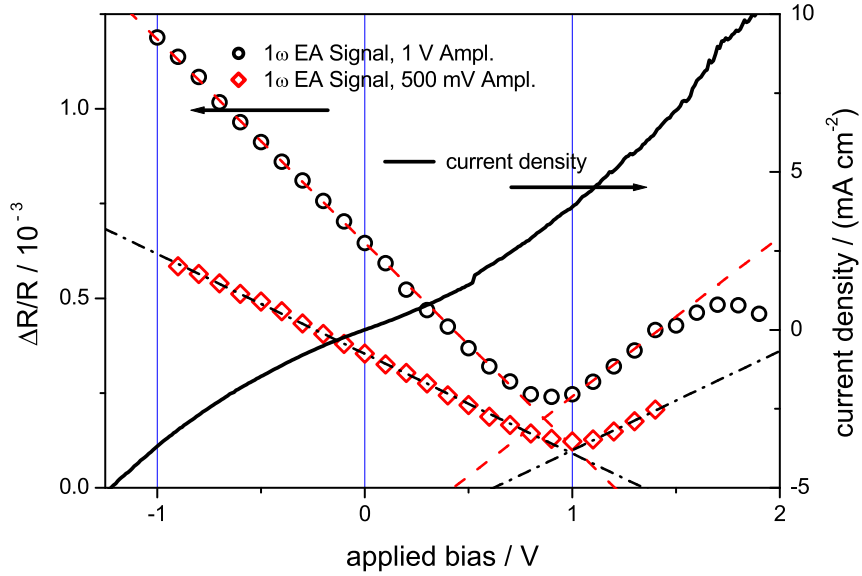


Figure 3.9: Internal electric field measurement and J-V curve at room temperature of an ITO - MDMO-PPV - LiF - Al device probed at 590 nm; 1 V amplitude (circles) and 500 mV (diamonds).

3.1.3 ITO - MDMO-PPV - LiF - Al Devices

Devices of the structure ITO - MDMO-PPV - LiF - Al with an active layer thickness of approximately 100 nm do not show any diode characteristic, which can be seen from the J-V curve in Fig. 3.9. The same figure also shows, that the 1ω EA signal of an ITO - MDMO-PPV - LiF - Al device at room temperature does not reach the zero level before increasing again. The curve measured with the higher amplitude is shifted to higher EA responses - even at the turning point. This behavior is similar to that of the ITO - MDMO-PPV - Al structure presented in Fig. 3.7.

Contrary to the ITO - MDMO-PPV - Al structure a few points of the rising branch obey a linear fit but the obtained straight lines clearly do not intersect the zero line at the same point.

After cooling down the device with liquid nitrogen, the internal electric field is determined to be 2 V (Fig. 3.10).

The Stark effect is zero at that voltage, no net electric field remains in the device.

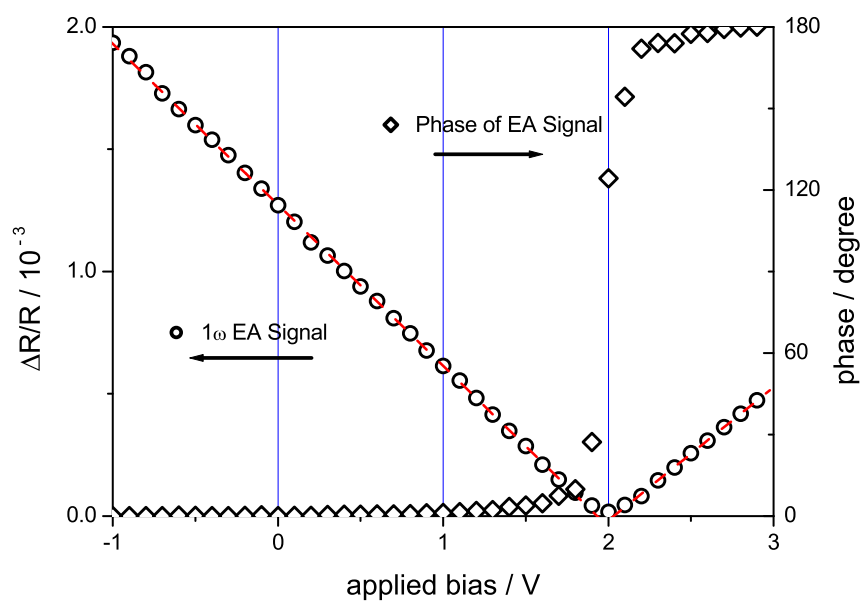


Figure 3.10: Internal electric field measurement and the phase of the 1ω EA signal at 77 K of an ITO - MDMO-PPV - LiF - Al device probed at 590 nm; 1 V amplitude.

3.1.4 ITO - PEDOT - MDMO-PPV - Al Devices

Introducing an interfacial layer of PEDOT:PSS into the device structure improves the J-V characteristic towards better rectification, as can be seen in Fig. 3.11. The reason is, that the PEDOT:PSS is so highly doped (compare Fig. 2.4) that it acts as electron blocking layer.

To determine the internal electric field, the 1ω EA response to the applied DC offset is observed. Even at room temperature the dependence is found to be linear over the whole measured range from -1 V to 2 V.

The declining branch from -1 V to 0.2 V can be fitted by a single formula, but for the rising branch two different slopes are observed. From 0.3 V where no Stark effect is observed to 1.1 V the EA response increases linearly with the applied voltage. From 1.2 V on the slope becomes steeper.

The AC amplitude for the measurement is 1 V peak-to-peak and the turn-on voltage roughly 1.5 V. The change in the fit formula therefore coincides with the threshold of current injection into the device. The meeting point of the two fits of the left and the right branch up to 1.1 V is 0.3 V. This voltage cancels the field inside the active layer.

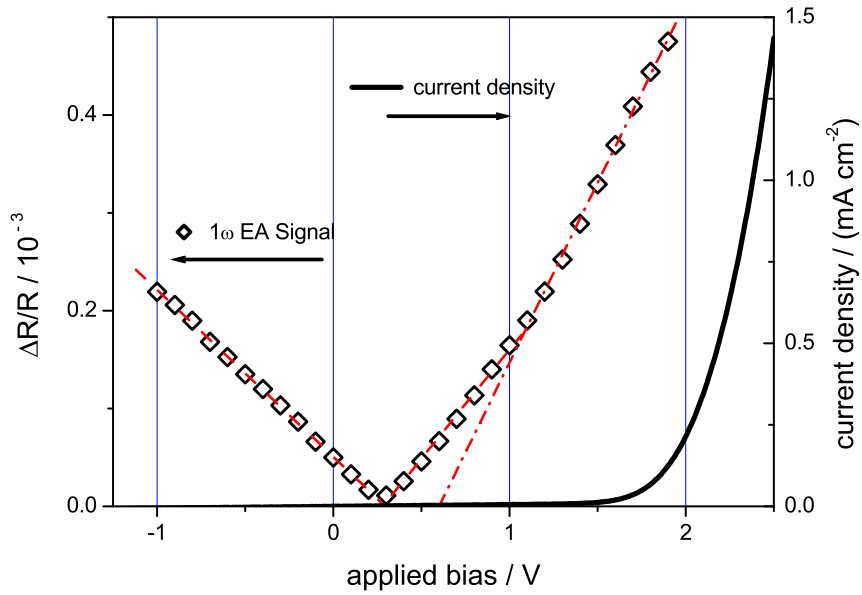


Figure 3.11: Internal electric field measurement and J-V curve at room temperature of an ITO - PEDOT - MDMO-PPV - Al device probed at 590 nm; 1 V amplitude.

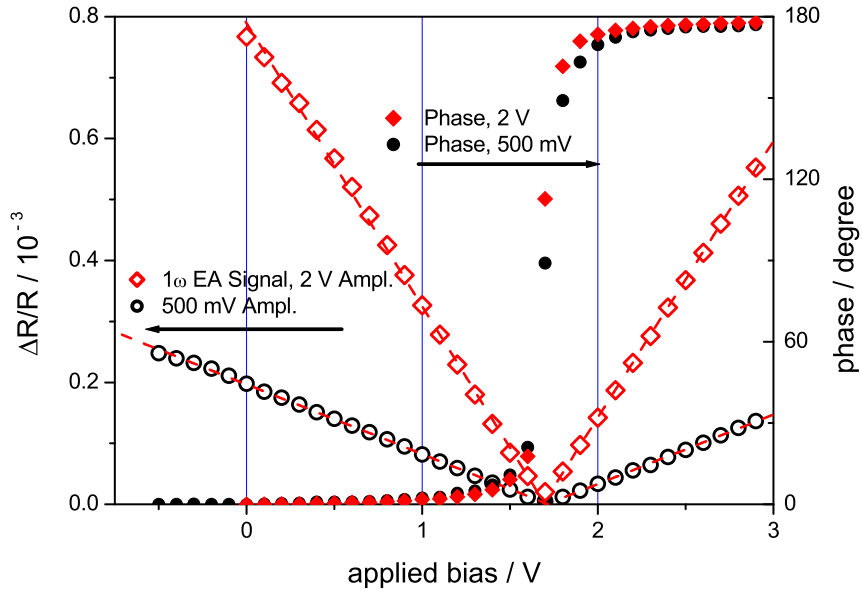


Figure 3.12: Internal electric field measurement and the phase of the 1ω EA signal at 77 K of an ITO - PEDOT - MDMO-PPV - Al device probed at 590 nm; 2 V amplitude (diamonds) and 500 mV amplitude (circles).

Repeating the same experiment at 77 K and with two different AC amplitudes, 500 mV and 2 V, the picture again looks very different. The voltage required to null the internal electric field is 1.7 V (Fig. 3.12).

3.1.5 ITO - PEDOT - MDMO-PPV - LiF - Al Devices

Also for the ITO - PEDOT - MDMO-PPV - LiF - Al structure a big discrepancy is observed between the internal electric field at room temperature and at 77 K.

Fig. 3.13 shows the data obtained from the determination of the internal electric field at room temperature. The linear fits of the two branches of the 1ω EA signal intersect the zero line at 0.25 V. To cancel the internal electric field and therefore the 1ω EA signal in an ITO - PEDOT - MDMO-PPV - LiF - Al structure at room temperature 0.25 V are necessary, at 77 K it takes 2 V (Fig. 3.14).

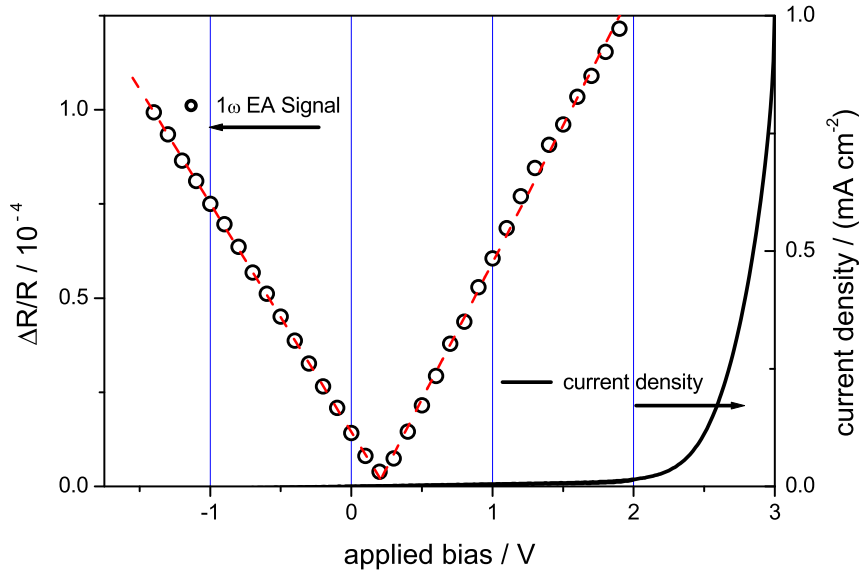


Figure 3.13: Internal electric field measurement and J-V curve at room temperature of an ITO - PEDOT - MDMO-PPV - LiF - Al device probed at 590 nm; 1 V amplitude.

3.1.6 Summary of the Results

Fig. 3.15 and Fig. 3.16 show the same plots as have been presented above. The figures summarize the graphs from which the values for the internal electric fields were obtained at room temperature and 77 K.

Table 3.1: Overview over the internal electric fields found in MDMO-PPV devices at room temperature and 77 K

Temperature	PPV	PEDOT PPV	PPV LiF	PEDOT PPV LiF
Room Temperature	1.1 V	0.3 V	1 V	0.2 V
77 K	1.6 V	1.7 V	2.0 V	2.0 V

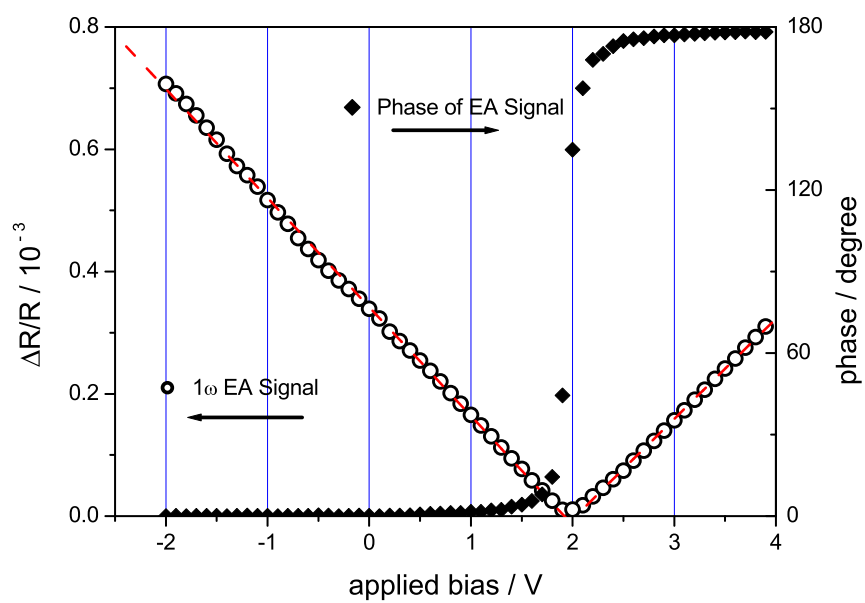


Figure 3.14: Internal electric field measurement and the phase of the 1ω EA signal at 77 K of an ITO - PEDOT - MDMO-PPV - LiF - Al device probed at 590 nm; 1 V amplitude.

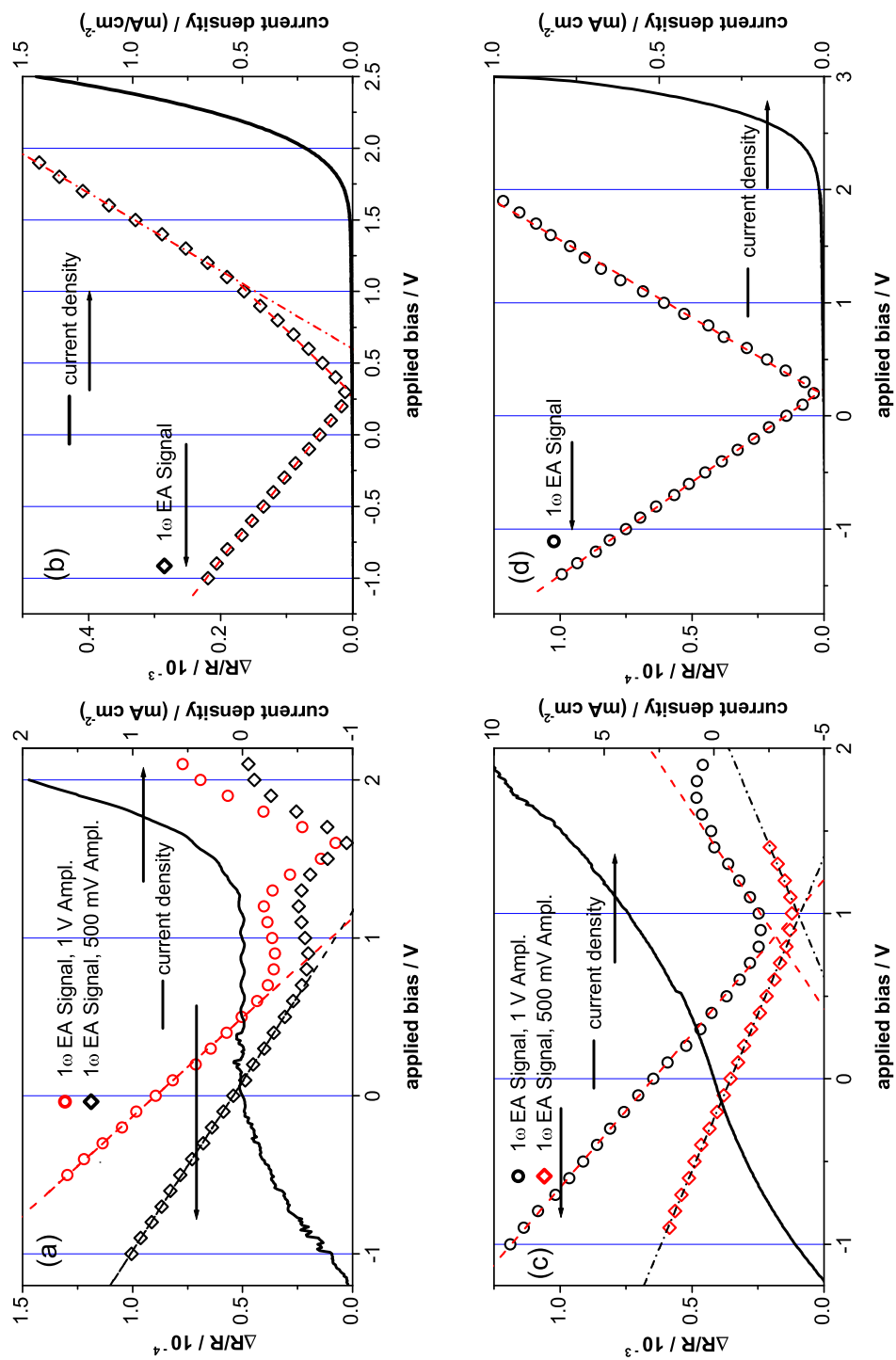


Figure 3.15: Layout of the plots obtained from internal electric field measurements at room temperature of the devices employing an active layer of MDMO-PPV. (a) ITO - MDMO-PPV - Al (b) ITO - PEDOT - MDMO-PPV - Al (c) ITO - MDMO-PPV - LiF - Al (d) ITO - PEDOT - MDMO-PPV - LiF - Al

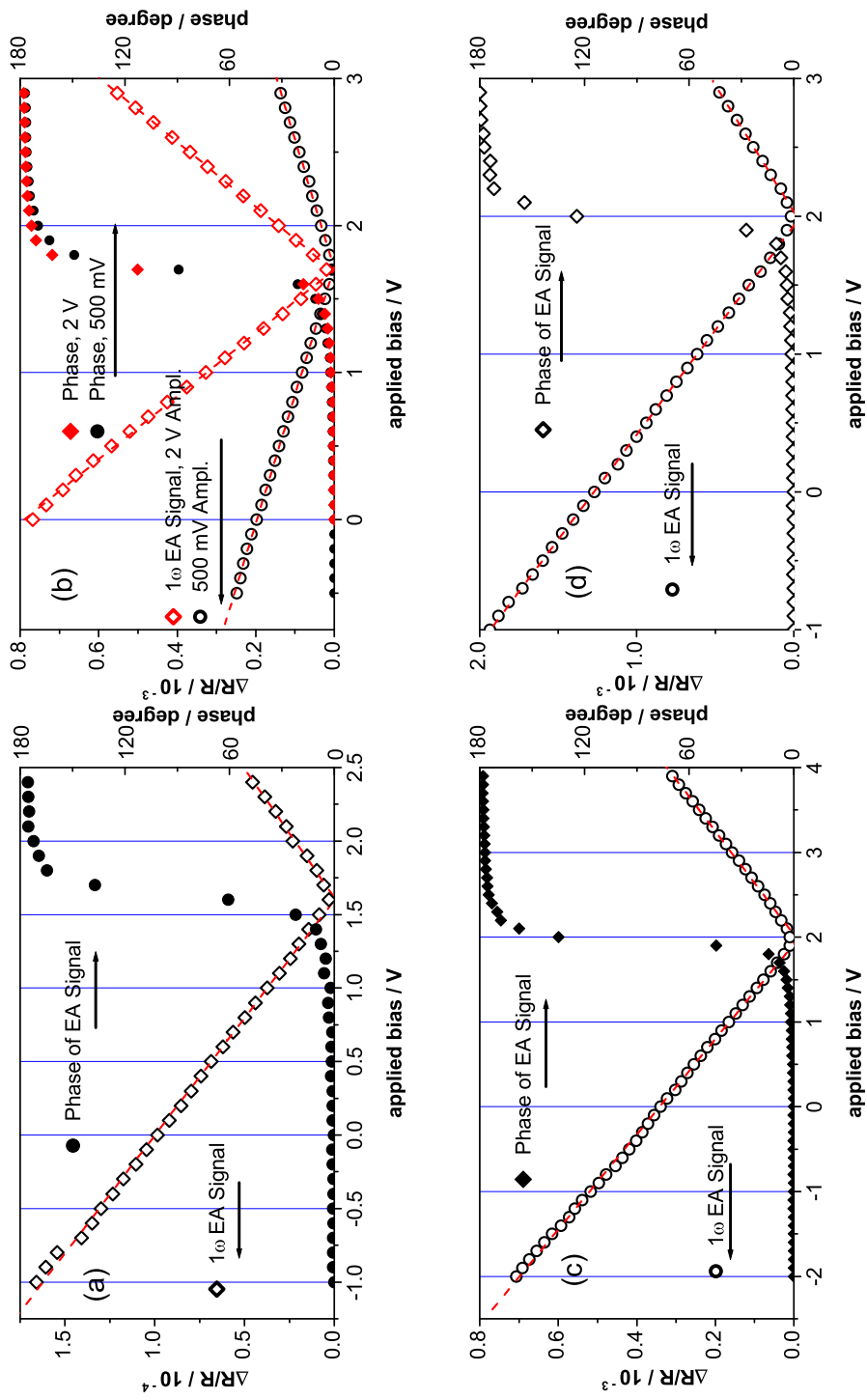


Figure 3.16: Layout of the plots obtained from internal electric field measurements at 77 K of the devices employing an active layer of MDMO-PPV. (a) ITO - MDMO-PPV - Al (b) ITO - PEDOT - MDMO-PPV - Al (c) ITO - PEDOT - MDMO-PPV - LiF - Al (d) ITO - MDMO-PPV - LiF - Al

3.2 P3HT Devices

This section focuses on devices employing an active layer of regioregular P3HT. The strategy is the same as for the study of MDMO-PPV devices shown above: ITO acts as anode and Al as cathode while the influence of interfacial layers such as PEDOT:PSS and LiF is investigated.

Fig. 3.17 shows the double path transmission spectrum and its first derivative of a 0.5 μm thick P3HT film sandwiched between ITO and Al.

Compared to MDMO-PPV, the P3HT absorbs at larger wavelengths, also shifting the region where electroabsorption is expected from 590 nm to around 650 nm.

In Fig. 3.18 the first harmonic (1ω) EA spectrum of an ITO - P3HT (400 nm) - Al device is compared with the first derivative of the double path transmission spectrum of the same sample. Below 700 nm the curves coincide equivalently well like those measured for MDMO-PPV (Fig. 3.3) and described in section 1.3.3. A slight discrepancy of the two peaks of about 10 nm can be observed. Around 710 nm a second peak arises in the 1ω EA spectrum, which is neither predicted by the first derivative of the double path transmission spectrum nor appears in the second harmonic (2ω) EA spectrum (Fig. 3.18). Just as in the case of devices employing MDMO-PPV as an active layer, this additional peak shows up adjacent to the main EA peak (Fig. 3.5). In thinner devices, this peak cannot be observed (compare Fig. 3.27).

In section 1.3.2, equation (1.14) describes the second harmonic EA signal scaling with the square of the AC amplitude but being independent of the applied DC offset and the internal electric field. Fig. 3.19 experimentally backs this prediction. From 2 V to 4 V, the maximum signal at 640 nm increases by a factor of four and from 2 V to 6 V by a factor of nine.

3.2.1 ITO - P3HT - Al Devices

ITO - P3HT - Al devices with an active layer of P3HT obtained from spin-casting of a 2% by weight solution of P3HT in chlorobenzene (as described in section 2.2.2) do not show any diode behavior. Due to the small layer thickness most of the current directly flows over shortcuts between ITO and the Al top electrode. Using a thin layer of LiF below the Al top contact allows to apply an electric field across the active layer.

Another way to avoid this problem is to prepare thicker active layers by using the doctor blade technique. For details check the section device preparation on page 13.

Devices of four different thicknesses, 200 nm, 400 nm, 500 nm and 1.3 μm were prepared for this inquiry.

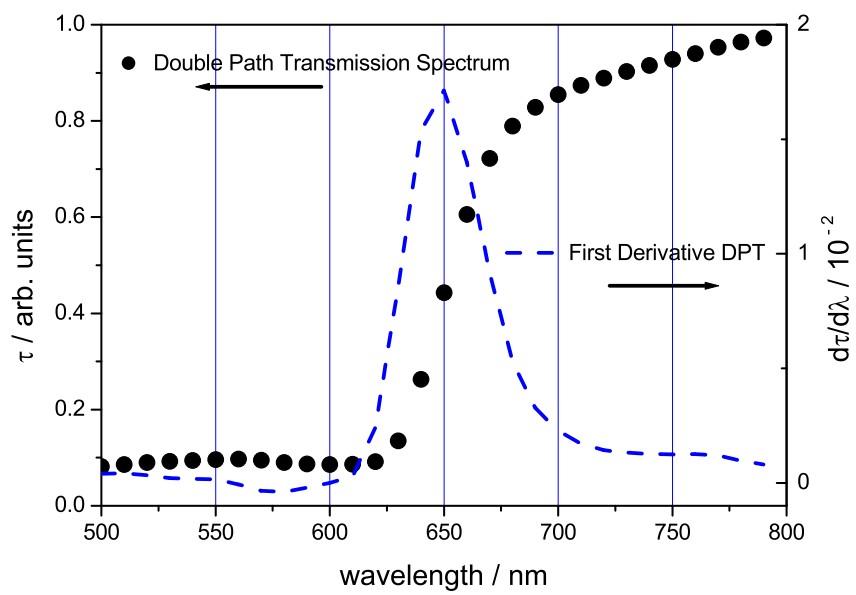


Figure 3.17: Double path transmission (DPT) spectrum and its first derivative of an ITO - P3HT ($\approx 0.5 \mu\text{m}$) - Al device measured at 77 K.

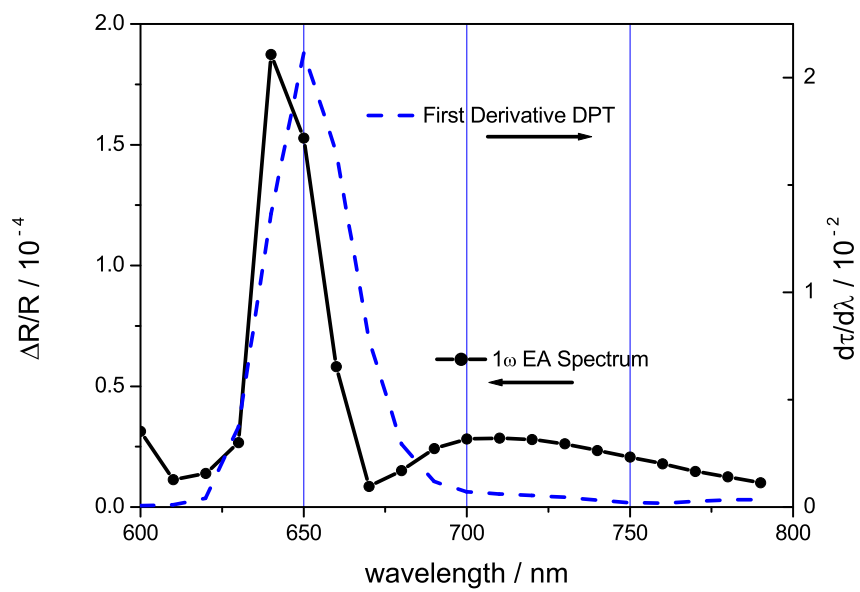


Figure 3.18: Comparison of the 1ω EA spectrum with the first derivative of the double path transmission (DPT) spectrum. ITO - P3HT (200 nm) - Al device measured at 77 K; -2 V offset, 2 V amplitude.

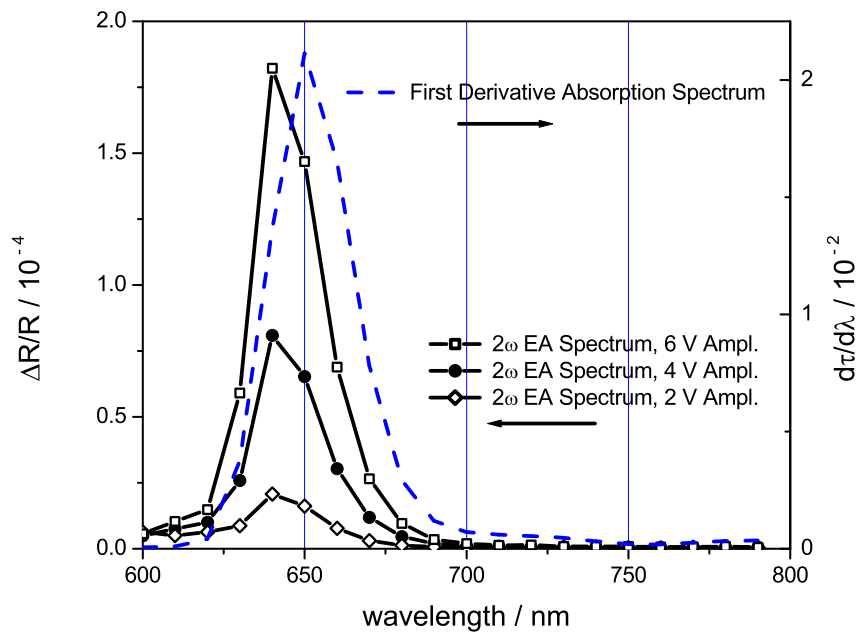


Figure 3.19: Second harmonic (2ω) EA spectrum of an ITO - P3HT (200 nm) - Al device measured at 77 K; -2 V offset, 6 V amplitude (squares); -2 V offset, 4 V amplitude (circles) and -2 V offset, 2 V amplitude (diamonds).

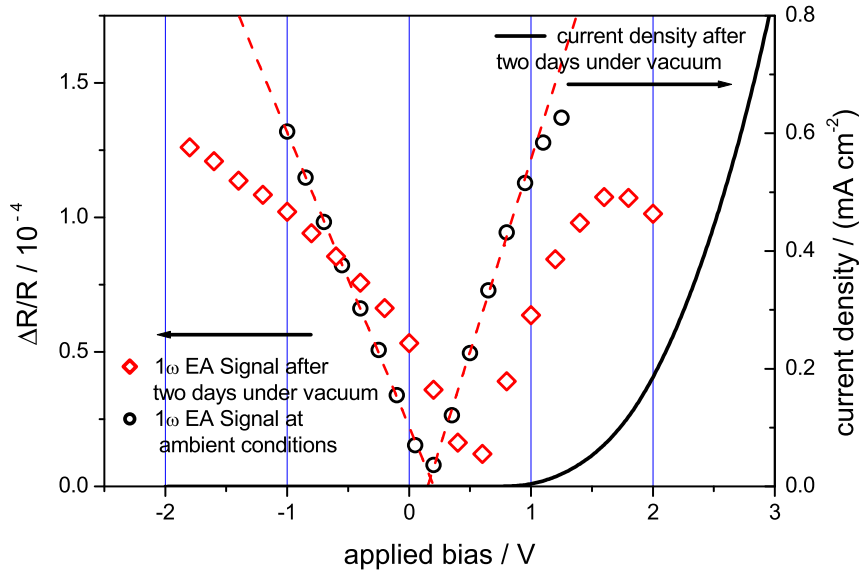


Figure 3.20: Internal electric field measurement and J-V curve measured at room temperature of an ITO - P3HT (200 nm) - Al device probed at 640 nm. Comparison of the results at ambient conditions (2 V amplitude, circles) with those obtained after two days under vacuum (2 V amplitude, diamonds).

200 nm thick P3HT Layer

The internal electric field of the structure ITO - P3HT (200 nm) - Al is measured at room temperature without evacuating the cryostat and found to be 0.2 V (Fig. 3.20). Below 1 V the falling and the rising branch can be fitted sensibly by a straight line. After two days under vacuum the internal electric field of the same device has risen to 0.5 V and the measured points do not obey a linear fit. The results are compared in Fig. 3.20.

A possible interpretation of this change in the internal electric field can be a reduction of the dopant concentration inside the active layer. Oxygen is known to improve the conductivity of P3HT films, an effect that can be revoked by keeping the films under vacuum.

The observation of reversible oxygen doping of P3HT is described in reference [27].

Upon cooling down the sample with liquid nitrogen, the internal electric field shifts to an even higher value: As can be seen in Fig. 3.21, the internal electric field is found to be ≈ 1.1 V.

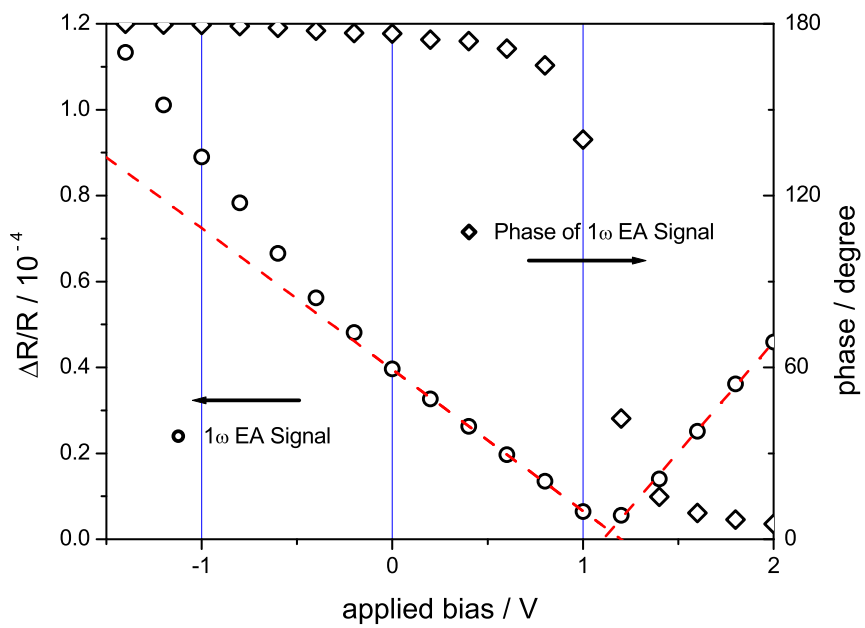


Figure 3.21: Internal electric field measurement and the phase of the 1ω EA signal measured at 77 K of an ITO - P3HT (200 nm) - Al device probed at 640 nm; 2 V amplitude.

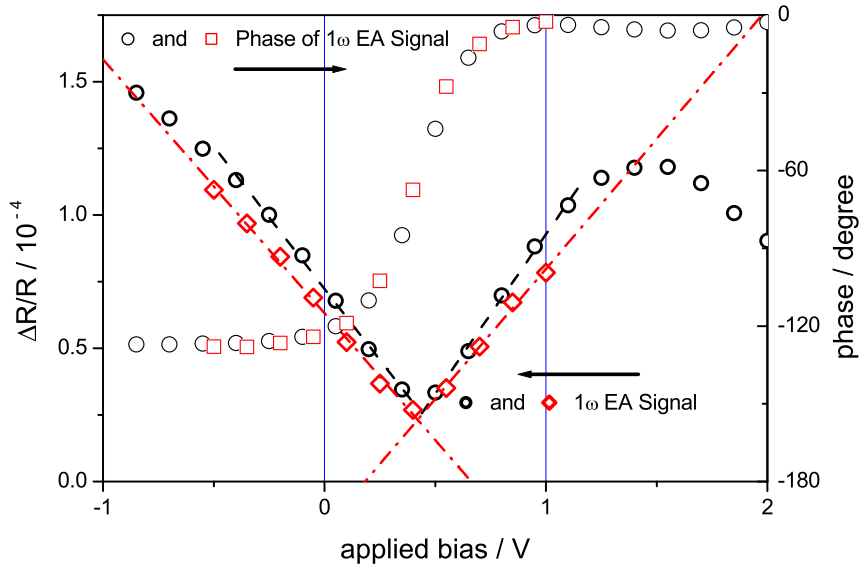


Figure 3.22: Internal electric field measurement at room temperature of an ITO - P3HT (400 nm) - Al device probed at 640 nm after 60 min (2 V amplitude, circles) and 150 min (2 V amplitude, diamonds) under vacuum, respectively.

400 nm thick P3HT Layer

After the installation into the cryostat a 400 nm thick P3HT device is kept under vacuum for about an hour, then the internal electric field is determined for the first time, after 2.5 hours for the second time. The results are shown in Fig. 3.22. Both times, the meeting point of the falling and the rising branch are located at the same applied voltage, but the EA signal at that point is not zero. This shows that the internal electric field does not change significantly on that timescale and can be determined to be 0.45 V. This value also resembles the internal electric field found for the depleted 200 nm thick P3HT device (Fig. 3.20) and just as in that case only a few points around the minimum at 0.45 V follow the linear fit.

500 nm thick P3HT Layer

Further evidence for effectively influencing the doping level in P3HT by reducing the pressure is found from the examination of an ITO - P3HT (500 nm) - Al structure with CELIV, electroabsorption and recording J-V curves. Immediately after installing the sample into the cryostat CELIV measurements were carried out and the J-V curve was recorded. The results of the

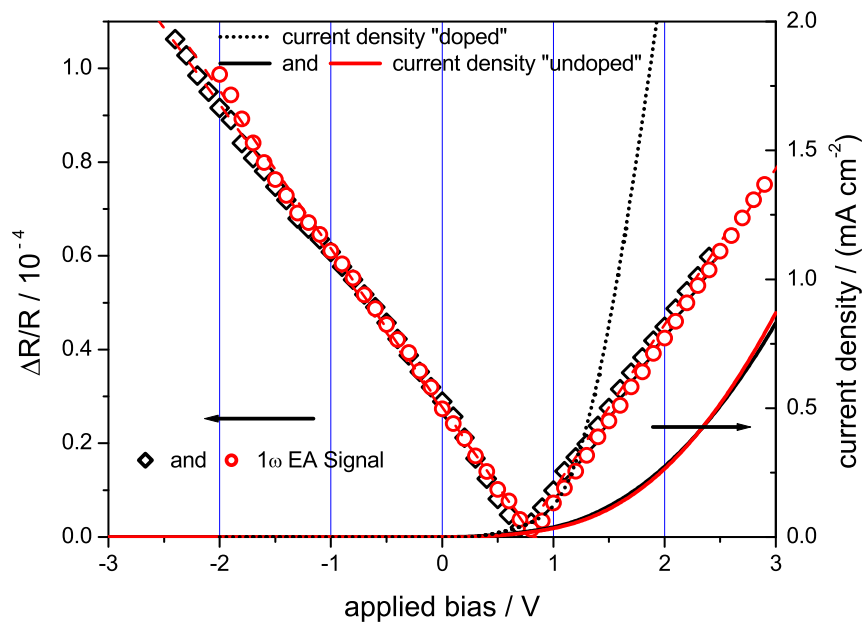


Figure 3.23: Comparison of the results of the internal electric field measurement and the J-V curve measured at room temperature of an ITO - P3HT (500 nm) - Al device probed at 640 nm: after 90 min (2.5 V amplitude, diamonds) under vacuum and an additional night under vacuum (2.5 V amplitude, circles). The dotted line represents the J-V curve at the initial doped state at ambient conditions.

CELIV can be directly related to the charge carrier concentration inside the active layer.

After evacuation for approximately 1.5 hours, the measurements were repeated. Applying 2 V, the observed current was about an order of magnitude smaller than before and the CELIV shows a much lower charge carrier concentration. In fact, the active layer can be considered as depleted. This is backed by the observation, that additional time under vacuum over night does neither alter the J-V curve nor the results obtained from the internal electric field measurement.

In Fig. 3.23 the internal electric field measurement and the corresponding J-V curve after 1.5 hours under vacuum and after an additional night under vacuum are presented. Additionally it shows the J-V curve of the device in the initial doped state displaying a current that is one order of magnitude larger but still has the same onset. Neither the internal electric field nor the slopes of the linear fits change significantly. The additional time under vacuum over night does not seem to alter the condition of the sample and supports the appraisal, that the polymer layer is fully depleted. Consequentially no free charge carriers are present inside the active layer, which could screen the electric field.

In the state where no further depletion of the active layer could be achieved by evacuation, the internal electric field in an ITO - P3HT (500 nm) - Al device is determined to be 0.8 V.

No low temperature experiments could be carried out using films thicker than 200 nm, because the thicker samples neither showed any conductivity nor could any Stark effect be observed at 77 K. Whatever the reason for this behavior is, the effect is reversible, because after defrosting the sample the J-V curve is the same as before.

1300 nm thick P3HT Layer

A 1.3 μm thick P3HT film with Al top contact was installed into the cryostat and evacuated until the pressure has reached approximately 10^{-4} mbar. Then the valve was closed to keep the vacuum at that level. The carrier concentration inside the active layer was determined using CELIV, which proofed the P3HT to be doped. Successively the internal electric field (compare section 1.3.2) was measured, first with 5 V amplitude, subsequently with 2.5 V. Because with increasing thickness the electric field strength across the active layer decreases and the EA signal scales with the square of the electric field these high amplitudes are necessary to get a reasonable EA response. CELIV measurements prove that the undoping process in this very thick device is much slower than it was in the 500 nm thick P3HT film. From Fig. 3.24 the internal electric field can be determined to be between 1.1 and 1.2 V.

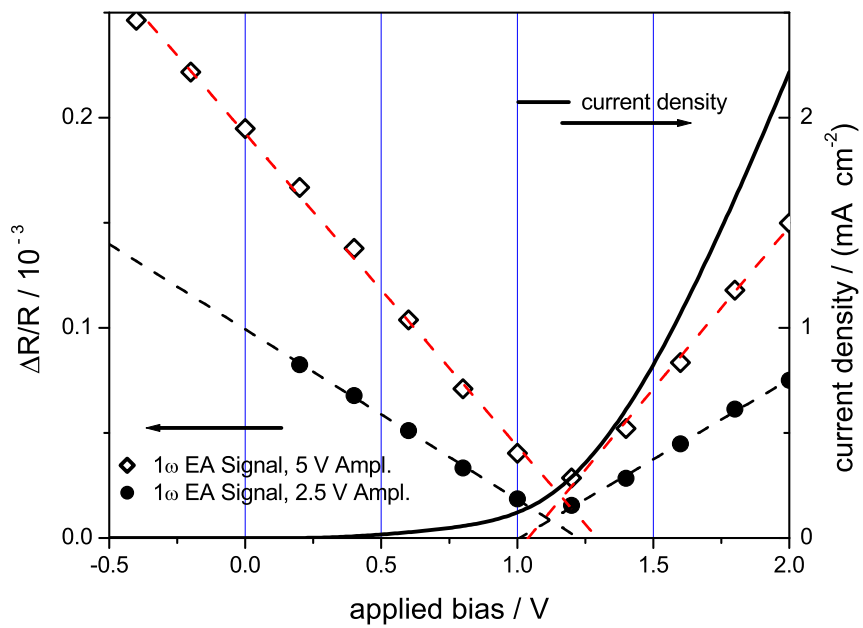


Figure 3.24: Internal electric field measurement and J-V curve measured at room temperature of a doped ITO - P3HT (1.3 μm) - Al device probed at 640 nm. 2.5 V (filled circles) and 5 V (open diamonds) amplitude.

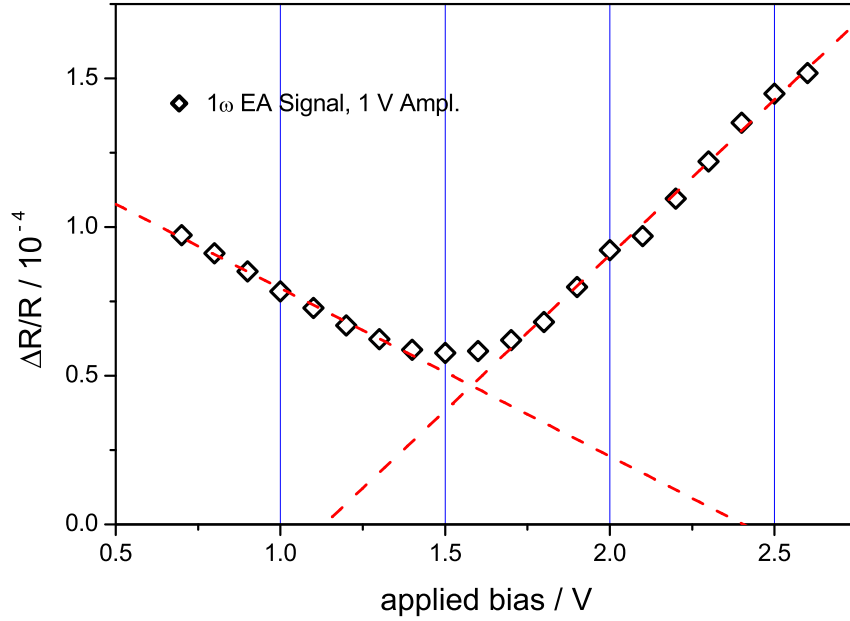


Figure 3.25: Internal electric field measurement at room temperature of an ITO - P3HT - LiF - Al device probed at 640 nm; 1 V amplitude.

3.2.2 ITO - P3HT - LiF - Al Devices

As mentioned above, devices with an active layer spin-coated from a 2% solution of P3HT in chlorobenzene directly onto ITO do not show rectifying behavior.

Implementing a 0.6 nm thick layer of LiF between the polymer and the Al top electrode allows to observe the Stark effect, when a certain bias is applied to the sample.

In the experiment to determine the internal electric field of an ITO - P3HT - LiF - Al device at room temperature (the results are shown in Fig. 3.25) the 1ω EA signal does not drop to zero at the minimum located at 1.6 V. Cooling down the sample to 77 K and repeating the experiment, the 1ω EA response is found to change linearly with the applied DC offset. The linear fits of the rising and the falling branch intersect the zero line at 1.7 V, where the EA response is measured to be almost zero. Also the characteristic of the phase of the lock-in signal shows perfect behavior. The phase remains constant when approaching the internal electric field from both sides and exactly at 1.7 V changes by 180 degrees. In Fig. 3.26 the results are displayed.

The current measured between the electrodes shows ohmic behavior even at

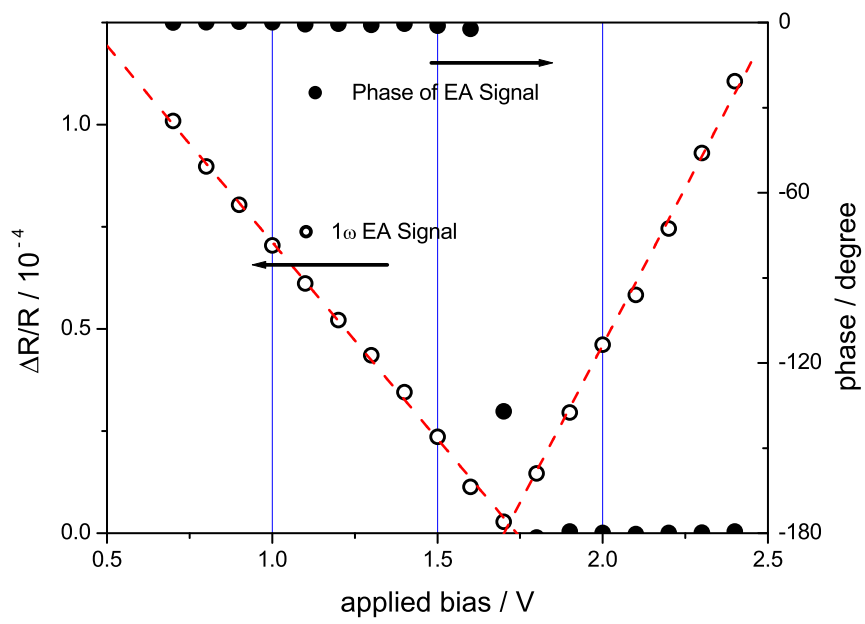


Figure 3.26: Internal electric field measurement and the phase of the 1ω EA signal measured at 77 K of an ITO - P3HT - LiF - Al device probed at 640 nm; 1 V amplitude.

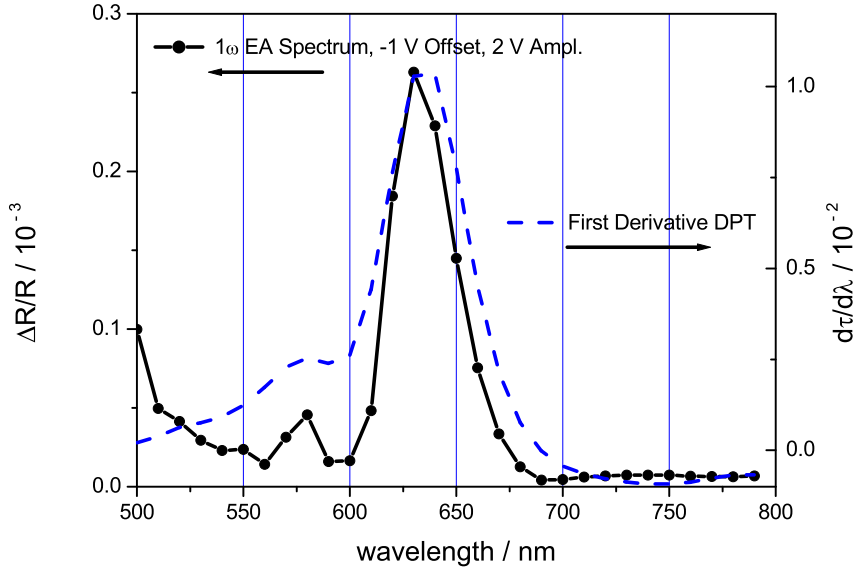


Figure 3.27: 1ω EA spectrum compared to the first derivative of the double path transmission (DPT) spectrum of an ITO - PEDOT - P3HT - Al device at room temperature; -1 V offset, 2 V amplitude.

77 K, but is reduced by an order of magnitude compared to room temperature. This fact is indicating some shortcuts between the electrodes carrying the current.

3.2.3 ITO - PEDOT - P3HT - Al Devices

Comparing the EA spectra of a thin ITO - PEDOT - P3HT (80 nm) - Al device displayed in Fig. 3.27 and Fig. 3.28 with the EA spectra of the ITO - P3HT (200 nm) - Al structure shown in Fig. 3.18 and Fig. 3.19 shows, that besides the dominating peak at 640 nm a second one around 580 nm becomes visible. This small peak at 580 nm can be seen because only about 80 nm of P3HT are used, therefore the device absorbs less light which allows to resolve the region below 600 nm and to observe the feature predicted by the first derivative of the double path transmission spectrum. On the other hand, the broad peak around 710 nm known from the 1ω EA spectrum of the 200 nm thick P3HT film (Fig. 3.18) does not show up in the thin device as can be seen in Fig. 3.27.

Just as it has been the case for the devices employing MDMO-PPV presented in section 3.1, by adding a layer of PEDOT:PSS between the ITO

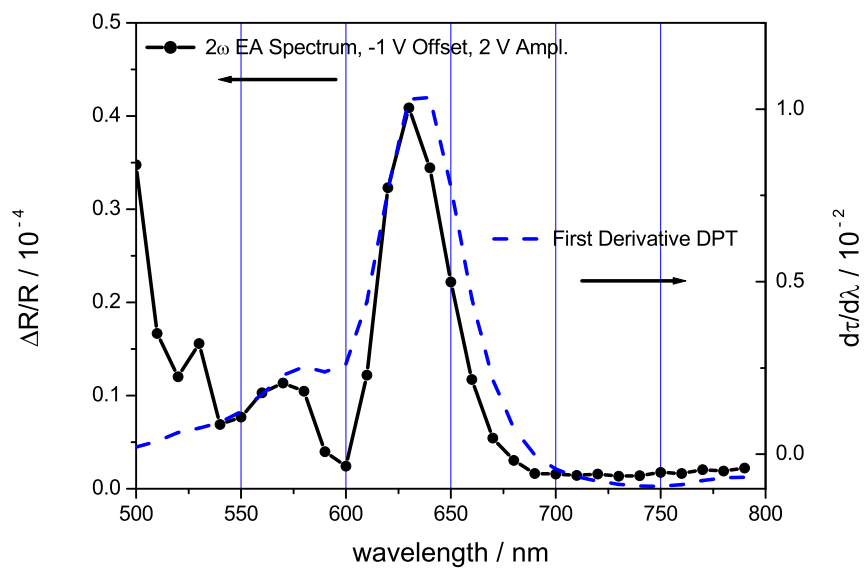


Figure 3.28: Second harmonic (2ω) EA spectrum compared to the first derivative of the double path transmission (DPT) spectrum of ITO - PEDOT - P3HT - Al device at room temperature. -1 V offset, 2 V amplitude.

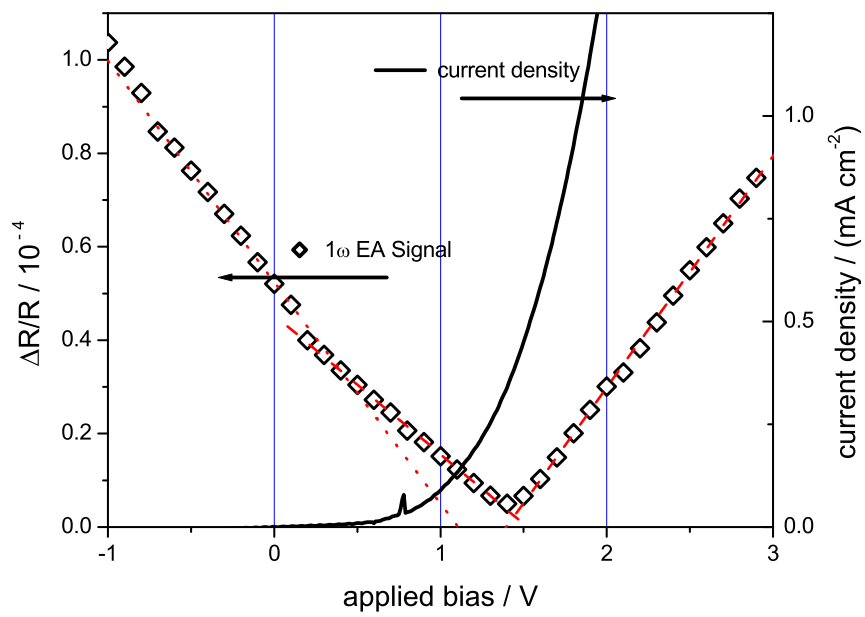


Figure 3.29: Internal electric field measurement and J-V curve measured at room temperature of an ITO - PEDOT - P3HT - Al device probed at 640 nm; 1 V amplitude.

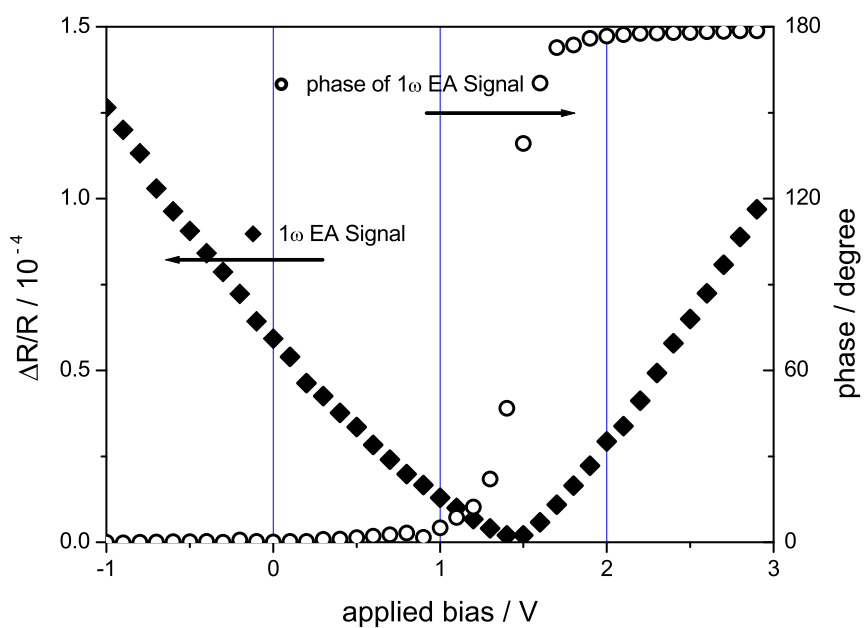


Figure 3.30: Internal electric field measurement and the phase of the 1ω EA signal measured at 77 K of an ITO - PEDOT - P3HT - Al device probed at 640 nm; 1 V amplitude.

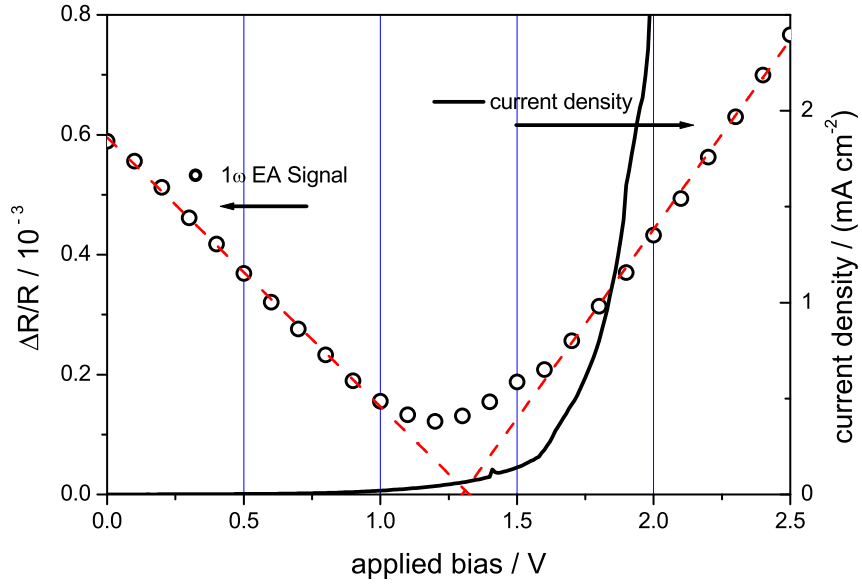


Figure 3.31: Internal electric field measurement and J-V curve at room temperature of an ITO - PEDOT - P3HT - LiF - Al device probed at 640 nm; 2 V amplitude.

on glass substrate and the polymer, the current rectifying property of the device is increased.

The J-V curve in Fig. 3.29 shows such an improved diode characteristic.

The EA response obtained from the device (Fig. 3.29) scales linearly with the applied DC bias, although the falling branch cannot be fitted by a single straight line. At approximately 0.2 V the slope changes. This point coincides with the threshold, when the DC offset plus the AC amplitude (1 V peak-to-peak) reaches into the injection part of the diode.

The dependence of the 1ω EA signal on the applied DC offset at 77 K in Fig. 3.30 does not seem to obey a linear fit formula at all, but the EA response drops to zero at 1.45 V.

3.2.4 ITO - PEDOT - P3HT - LiF - Al Devices

Introducing a layer of LiF does not increase the internal electric field at room temperature. The extrapolated branches in Fig. 3.31 exactly intersect the zero line at 1.3 V.

At 77 K, the internal electric field of the ITO - PEDOT - P3HT - LiF - Al structure is found to be slightly higher than without the LiF layer.

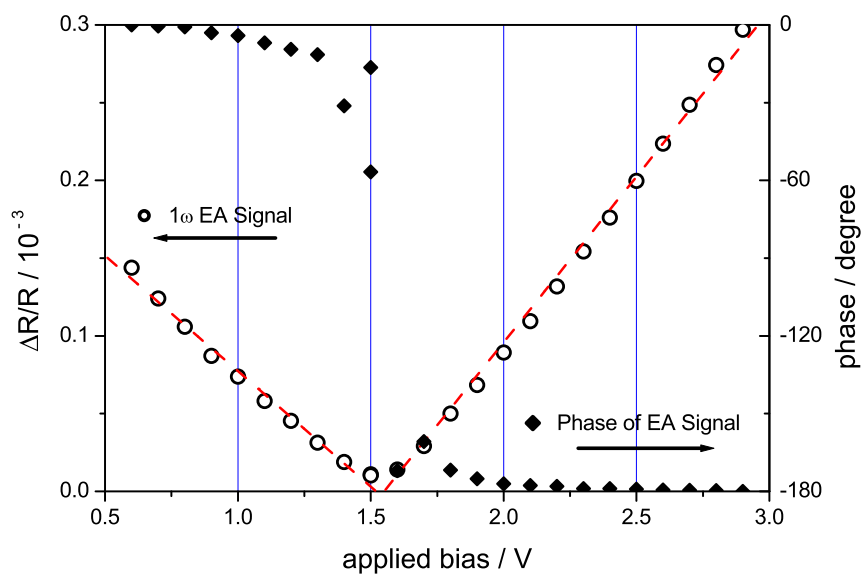


Figure 3.32: Internal electric field measurement and the phase of the 1ω EA signal at 77 K of an ITO - PEDOT - P3HT - LiF - Al device probed at 640 nm; 3 V amplitude.

Table 3.2: Overview over the values obtained for the internal electric field found in P3HT devices of various thicknesses at room temperature and 77 K.

	200 nm P3HT	400 nm P3HT	500 nm P3HT	1300 nm P3HT
Room Temp.	0.5 V	0.4 V	0.8 V	1.1 V
77 K	1.1 V	-	-	-

Table 3.3: Overview over the values obtained for the internal electric field of 80 nm thick P3HT devices at room temperature and 77 K.

	PEDOT P3HT	P3HT LiF	PEDOT P3HT LiF
Room Temp.	1.4 V	1.6 V	1.3 V
77 K	1.45 V	1.7 V	1.5 V

The points in Fig. 3.32 were determined in two experiments on the same sample, one going from 0.6 V to 1.5 V and the other from 1.5 V to 3 V. Therefore the course of the phase does not run smoothly over the whole range, but it is clearly shown that the phase changes significantly around 1.5 V, representing the internal electric field.

3.2.5 Summary of the Results

In this section the results presented above are summarized to show a condensed overview over the obtained findings.

Fig. 3.33 and Table 3.2 comprise the results of the experiments on the ITO - P3HT - Al devices of various thicknesses. The graphs used for the determination of the internal electric field at room temperature are pooled in Fig. 3.33.

Fig. 3.34, Fig. 3.35 and Table 3.3 give an overview over the results of the internal electric field measurements done on the P3HT devices employing interfacial layers of PEDOT:PSS and LiF.

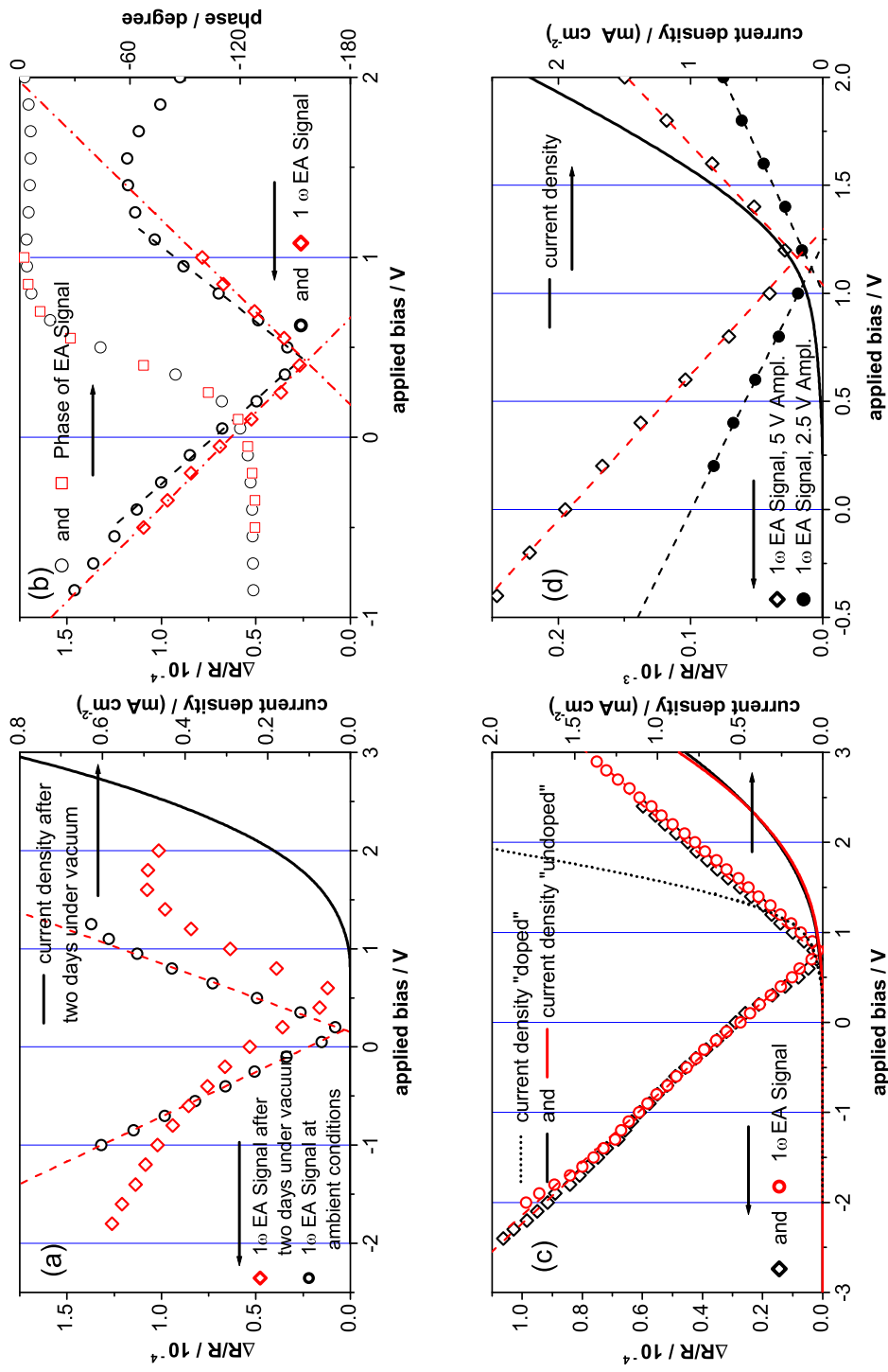


Figure 3.33: Layout of the plots obtained from internal electric field measurements at room temperature of ITO - P3HT - Al devices of various thicknesses. (a) ITO - P3HT (200 nm) - Al (b) ITO - P3HT (400 nm) - Al (c) ITO - P3HT (500 nm) - Al (d) ITO - P3HT (1300 nm) - Al

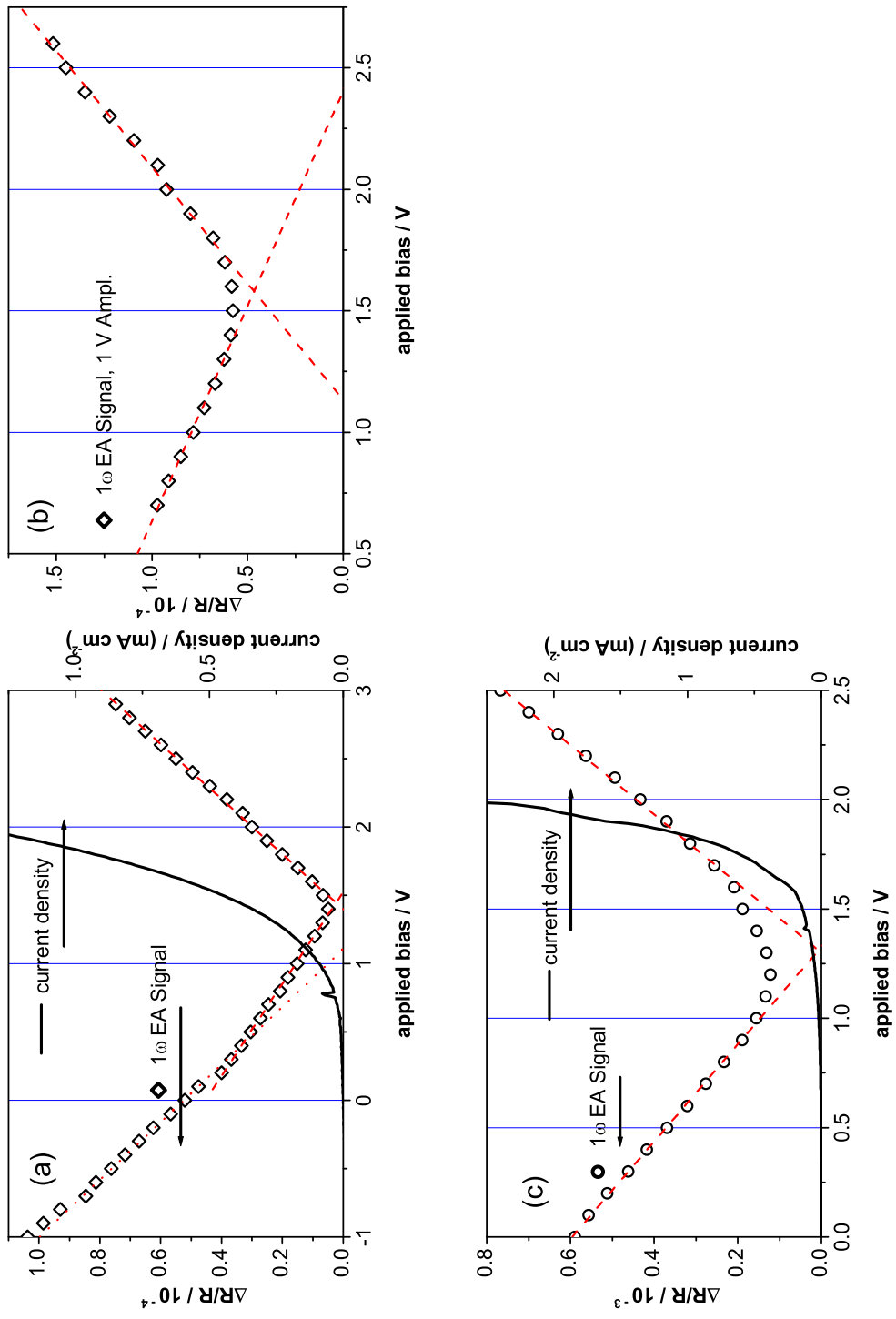


Figure 3.34: Layout of the plots obtained from internal electric field measurements at room temperature of the devices employing an active layer of P3HT. (a) ITO - PEDOT - P3HT - Al (b) ITO - P3HT - LiF - Al (c) ITO - PEDOT - P3HT - Al.

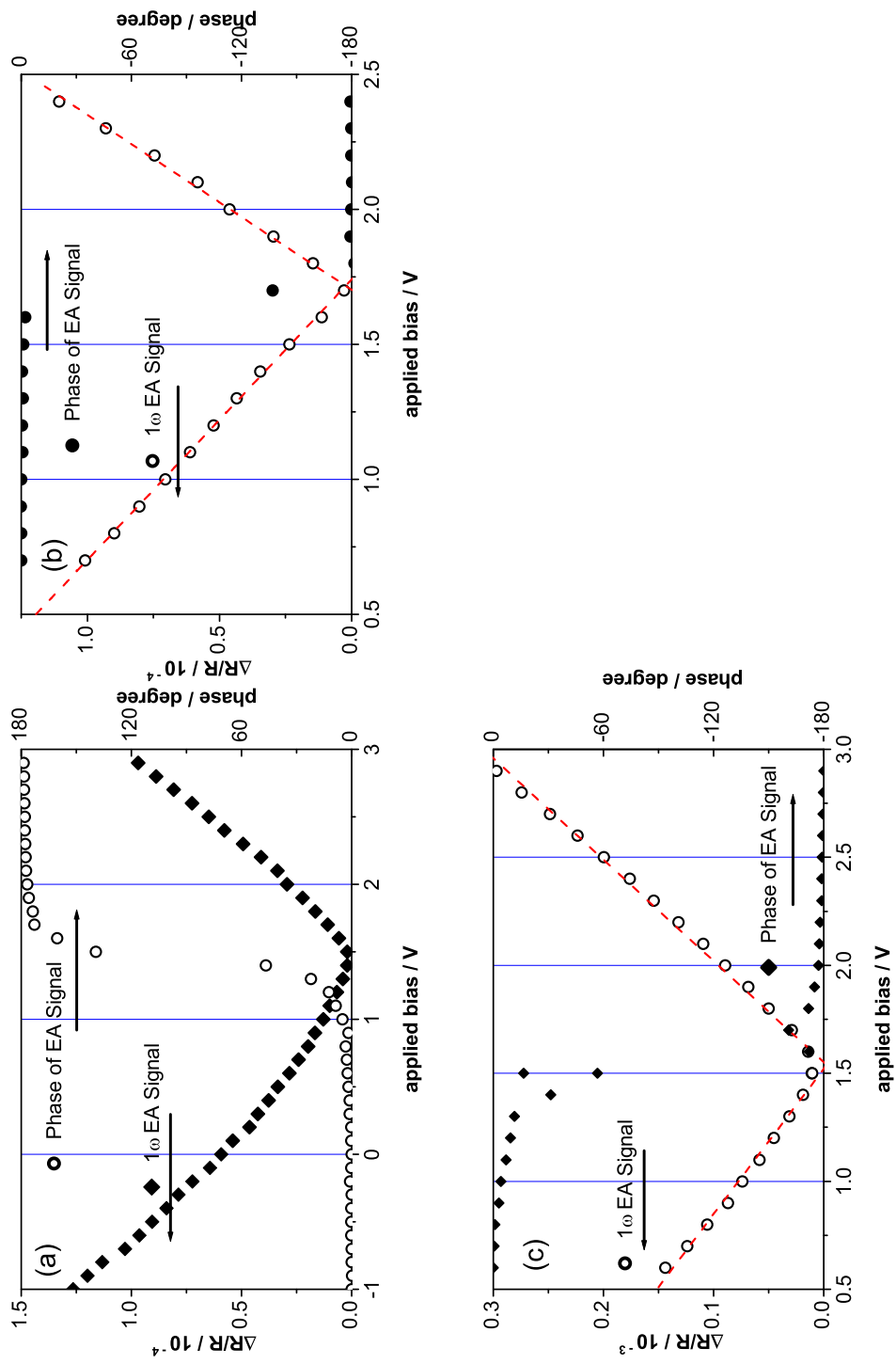


Figure 3.35: Layout of the plots obtained from internal electric field measurements at 77 K of the devices employing an active layer of P3HT. (a) ITO - PEDOT - P3HT - Al (b) ITO - PEDOT - P3HT - LiF - Al (c) ITO - PEDOT - P3HT - LiF - Al.

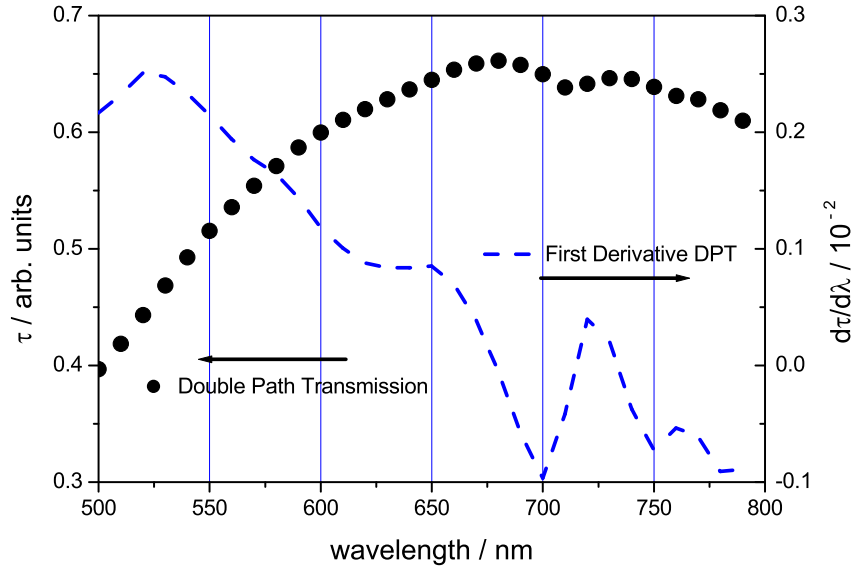


Figure 3.36: Double path transmission (DPT) spectrum of an ITO - PEDOT - PCBM - LiF - Al structure and its first derivative at 77 K.

3.3 PCBM Devices

Diodes with an active layer of PCBM were prepared by spin-coating a 3% by weight solution of PCBM in chlorobenzene onto a PEDOT:PSS covered ITO on glass substrate. A thin layer of LiF and a reflecting Al electrode were evaporated on top. Details concerning the device preparation are found in the section 2.2 on page 13.

Fig. 3.36 shows the double path transmission spectrum and its first derivative of the ITO - PEDOT - PCBM - LiF - Al device at 77 K. The sample absorbs poorly in the visible range and has a brownish color.

In Fig. 3.37 the J-V curves of the device at low temperature and room temperature are compared. Fig. 3.38 displays the same data plotted in logarithmic scale.

The diodes with an active layer made of PCBM show a big difference in the J-V characteristic compared to the devices employing a layer of a conductive polymer. By cooling down the polymer to 77 K, the amount of current that is transported is reduced dramatically and the device loses its rectifying behavior.

This is not the case for PCBM diodes. Upon cooling down, the onset of the current injection is shifted to higher voltages and the line shape of the

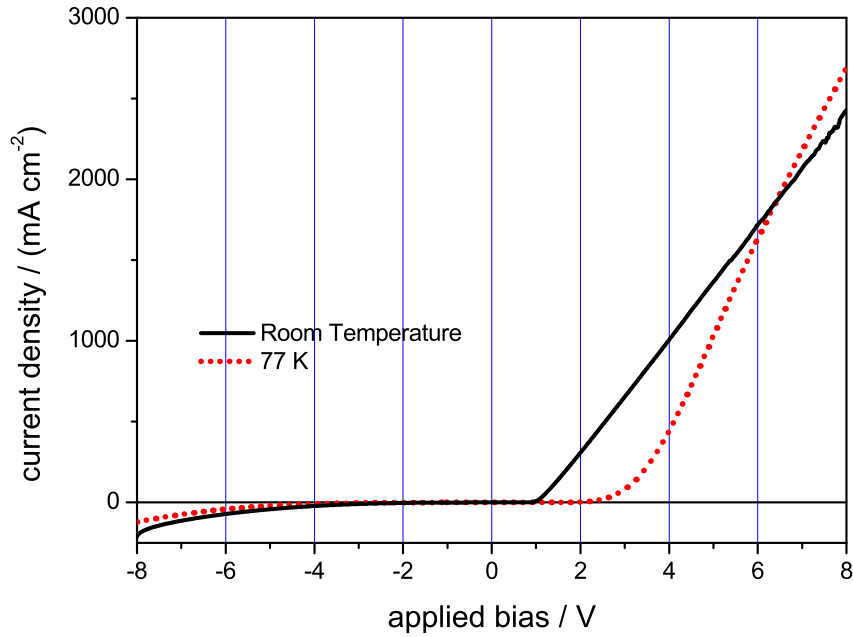


Figure 3.37: Comparison of the J-V characteristics of the ITO - PEDOT - PCBM - LiF - Al devices at room temperature (solid curve) and at 77 K (dotted curve).

J-V curve changes, but the device is still a diode: At 2 V the charge density does not even reach one percent of the amount observed at room temperature but from approximately 7 V on, the current at low temperature exceeds the current at room temperature.

The injection part of the J-V characteristic at room temperature shows linear behavior (Fig. 3.37). This represents ohmic transport and therefore a constant concentration of mobile charge carriers over the entire thickness of the film. Cooling down the sample with liquid nitrogen significantly changes the nature of current conduction to space charge limited transport indicated by the exponential onset of the J-V characteristic in Fig. 3.37.

By comparing the 2ω EA spectrum with the first derivative of the double path transmission spectrum another difference between the devices made with polymer and with PCBM becomes obvious.

The EA spectra of MDMO-PPV (Fig. 3.4) and P3HT (Fig. 3.19) nicely confirm the line shape predicted by the first derivative of the double path transmission spectra whereas the agreement of the two curves in the case of

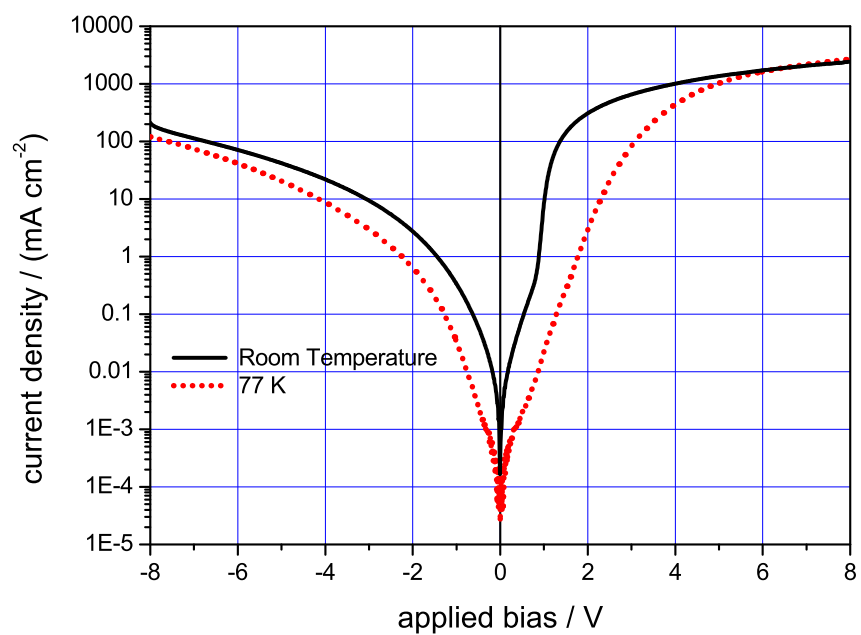


Figure 3.38: J-V characteristics of the ITO - PEDOT - PCBM - LiF - Al devices at room temperature (solid curve) and at 77 K (dotted curve) in a logarithmic plot.

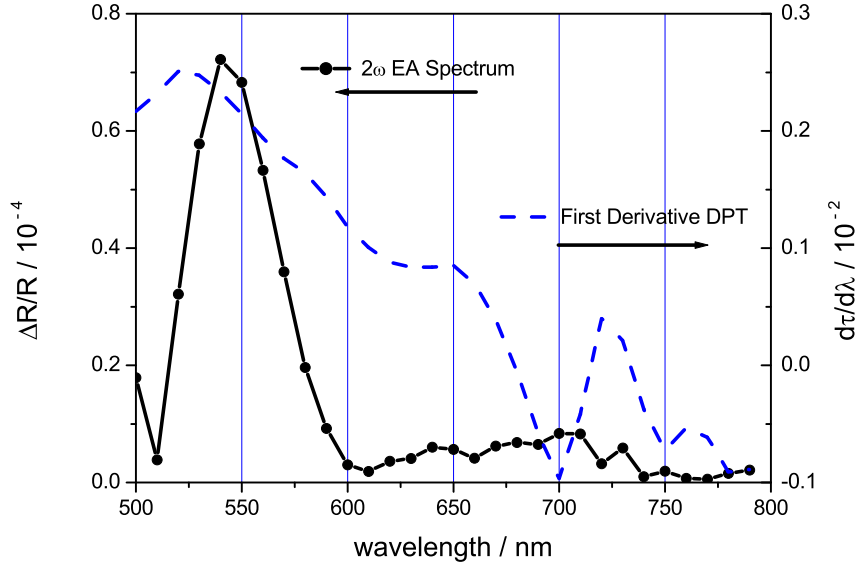


Figure 3.39: The second harmonic (2ω) EA spectrum compared to the first derivative of the double path transmission (DPT) spectrum of an ITO - PEDOT - PCBM - LiF - Al device measured at 77 K; -1 V offset, 2.5 V amplitude.

PCBM is only poor.

The validity of the mathematical treatment presented in section 1.3.3 is based on the assumption that the ground state and the first excited state of the studied material are of different parity, which is necessary to observe an allowed transition between these two energy levels. This case is shown in Fig. 1.1 and is valid for the luminescent polymers. In the case of fullerenes, the ground state and the first excited state are of the same parity [28]. Therefore an EA spectrum following the line shape of the first derivative of the unperturbed double path transmission spectrum is neither expected nor observed.

The first derivative of the DPT (Fig. 3.36) exhibits a broad spectral feature around 520 nm with a distinct shoulder at 650 nm, but in the second harmonic EA spectrum (Fig. 3.39) only one well resolved EA peak at 540 nm is observed. This most pronounced 1ω EA response is used to determine the internal electric field present in the PCBM layer. Probing at 550 nm and observing the change of the EA signal with the applied DC offset leads to the results shown in Fig. 3.40. The linear fit of the 1ω EA response intersects the zero line between 1 and 1.1 V. This result is found for the experiment at 77 K as well as at room temperature because both curves

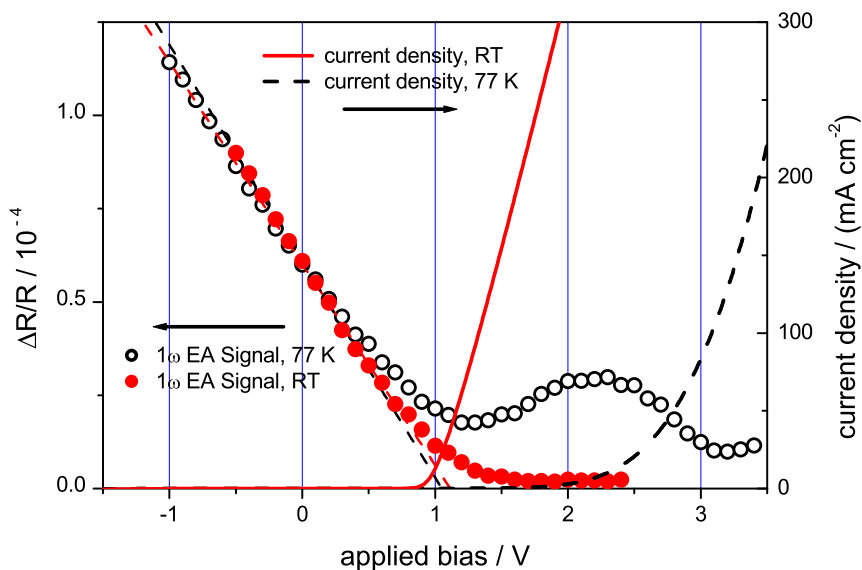


Figure 3.40: Plots comparing the internal electric field measurements of an ITO - PEDOT - PCBM - LiF - Al device at room temperature and 77 K; probed at 550 nm; 2 V amplitude.

almost coincide in reverse direction although they show a pronounced difference in forward direction. At room temperature, the EA signal drops to zero once the current injection regime is entered. The disappearance of the 1ω EA response above the turn-on voltage has been observed before in room temperature experiments on PLEDs and was ascribed to the screening of the internal electric field due to current injection [29].

At 77 K the course of the 1ω EA response with positive applied bias is not straight forward. The signal does not even reach zero, when the current density reaches values comparable to those at room temperature below 1.5 V. It even increases between 1.3 V and 2.3 V and slowly decreases again afterwards.

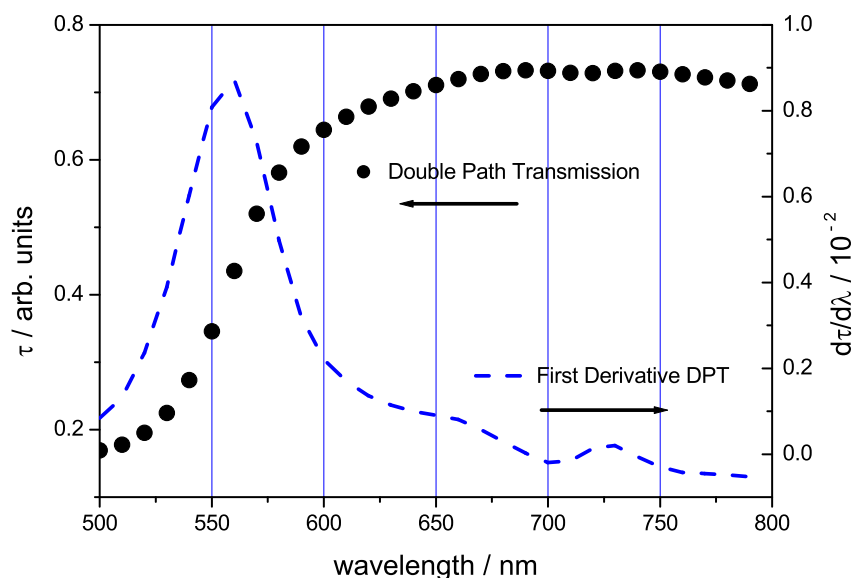


Figure 3.41: Double path transmission (DPT) spectrum of an ITO - PEDOT - MDMO-PPV/PCBM (1:4 in chlorobenzene) - LiF - Al device at room temperature and its first derivative.

3.4 MDMO-PPV/PCBM Blends

3.4.1 MDMO-PPV/PCBM Blends from Chlorobenzene

The weight ratio between polymer and acceptor molecule in the active layer of the MDMO-PPV/PCBM solar cells is 1:4. For details on the production process see page 14.

The double path transmission spectrum of an ITO - PEDOT - MDMO-PPV/PCBM (1:4 in chlorobenzene) - LiF - Al device shown in Fig. 3.41 looks very similar to that of the diodes employing only PCBM (Fig. 3.36), but the blend shows a sharper rise of the transmission around 550 nm due to the higher absorption of MDMO-PPV in that wavelength region. This leads to a more distinct and well resolved peak in the first derivative around 560 nm. As Fig. 3.42 and Fig. 3.43 show, the first harmonic EA spectra obtained at room temperature and 77 K are in good agreement with the first derivative of the double path transmission spectrum.

Probing the sample at the wavelength of the maximum 1ω EA response allows to determine the internal electric field. In reverse direction the 1ω EA signal scales linearly with the applied DC bias (Fig. 3.44), but once the DC offset plus the AC amplitude overshoot the turn-on voltage, the 1ω EA

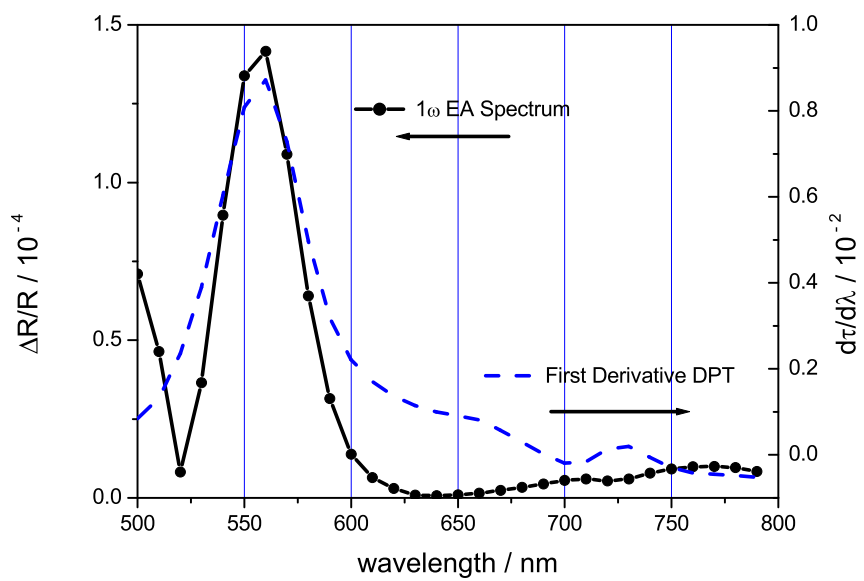


Figure 3.42: First harmonic (1ω) EA spectrum of an ITO - PEDOT - MDMO-PPV/PCBM (1:4 in chlorobenzene) - LiF - Al device measured at room temperature compared with the first derivative of the double path transmission (DPT) spectrum. -2 V offset, 1 V amplitude.

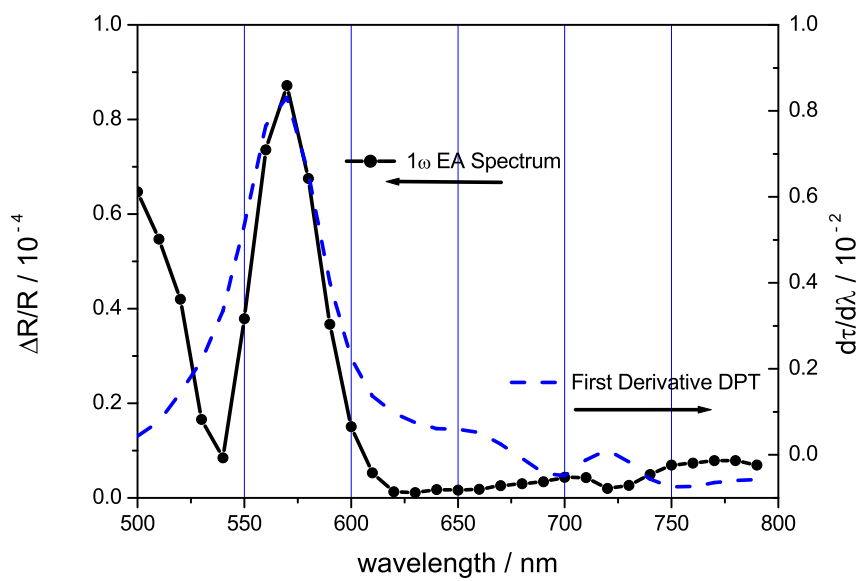


Figure 3.43: First harmonic (1ω) EA spectrum of an ITO - PEDOT - MDMO-PPV/PCBM (1:4 in chlorobenzene) - LiF - Al device measured at 77 K compared with the first derivative of the double path transmission (DPT) spectrum.

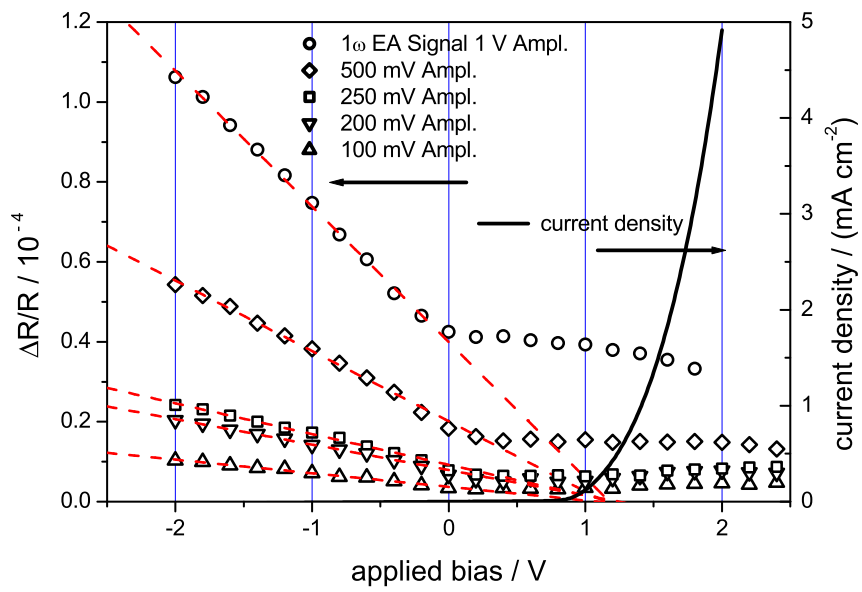


Figure 3.44: Internal electric field measurement and the J-V curve of an ITO - PEDOT - MDMO-PPV/PCBM (1:4 in chlorobenzene) - LiF - Al device at room temperature probed at 570 nm; The AC amplitude varies from 100 mV to 1 V.

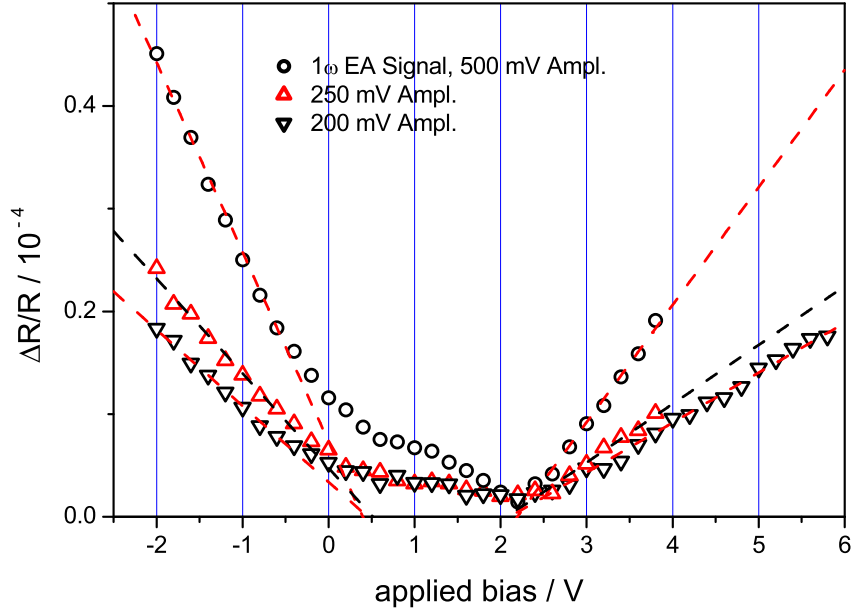


Figure 3.45: Internal electric field measurement and the J-V curve of an ITO - PEDOT - MDMO-PPV/PCBM (1:4 in chlorobenzene) - LiF - Al device at 77 K probed at 570 nm; The AC amplitude varies from 200 mV to 500 mV.

response remains almost independent of a further increase of the applied bias.

For all measured AC amplitudes the linear fits of the results obtained with reverse bias intersect the zero line at approximately 1.1 V.

Cooling down the sample to 77 K freezes out the injection current. The device loses its diode characteristic and also the increase of the 1ω EA signal with increasing forward bias can be observed. The points measured in reverse direction can be fitted linearly resulting in a point of intersection of the fit curves with the zero line at approximately 0.5 V. As can be seen in Fig. 3.45 the points measured in forward direction significantly deviate from these straight lines. At 2.2 V the EA response is almost equal to zero before rising again.

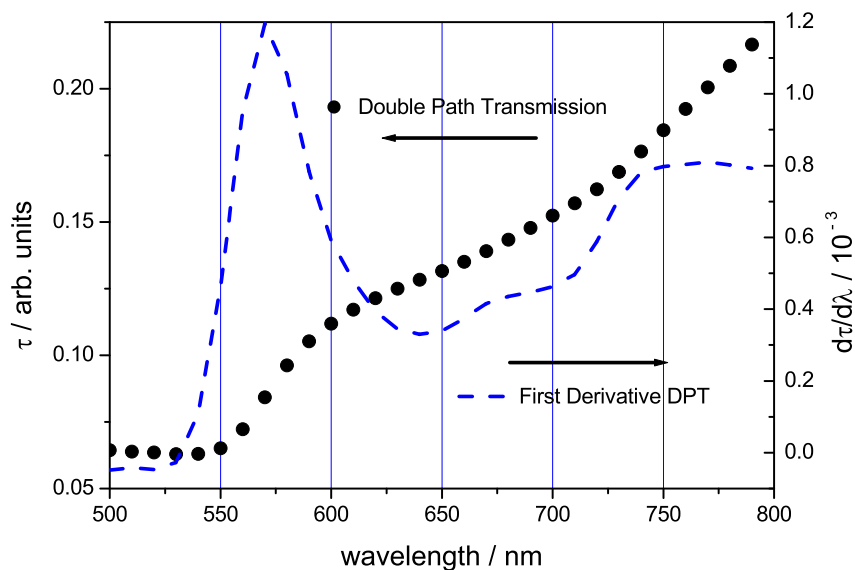


Figure 3.46: Double path transmission (DPT) spectrum of an ITO - PEDOT - MDMO-PPV/PCBM (1:4 in toluene) - LiF - Al device at room temperature and its first derivative.

3.4.2 MDMO-PPV/PCBM Blends from Toluene

The sample preparation is exactly the same as for the devices employing chlorobenzene, besides using toluene as the solvent.

Macroscopically, the spin-coated films from toluene are not as smooth as those cast from chlorobenzene, therefore the light reflected from the Al counter electrode is more diffuse. Less light can be collected by the lenses and focussed on the detector, resulting in a smaller signal than expected (Fig. 3.46).

Detailed studies on the surfaces using atomic force microscopy (AFM) showed a difference in the roughness of MDMO-PPV/PCBM films from toluene and chlorobenzene. Detailed results are found in reference [30].

Just as the MDMO-PPV/PCBM films cast from a solution in chlorobenzene, the films made from toluene show a peak around 570 nm in the first derivative of the double path transmission spectrum. Additionally the transmission increases again at wavelengths longer than 700 nm (Fig. 3.46) resulting in a broad feature in the first derivative, that cannot be seen in the case of chlorobenzene (Fig. 3.41).

Even the first harmonic (1ω) EA spectrum (Fig. 3.47) of the toluene cast films is richer than that of the chlorobenzene cast films (Fig. 3.42), contain-

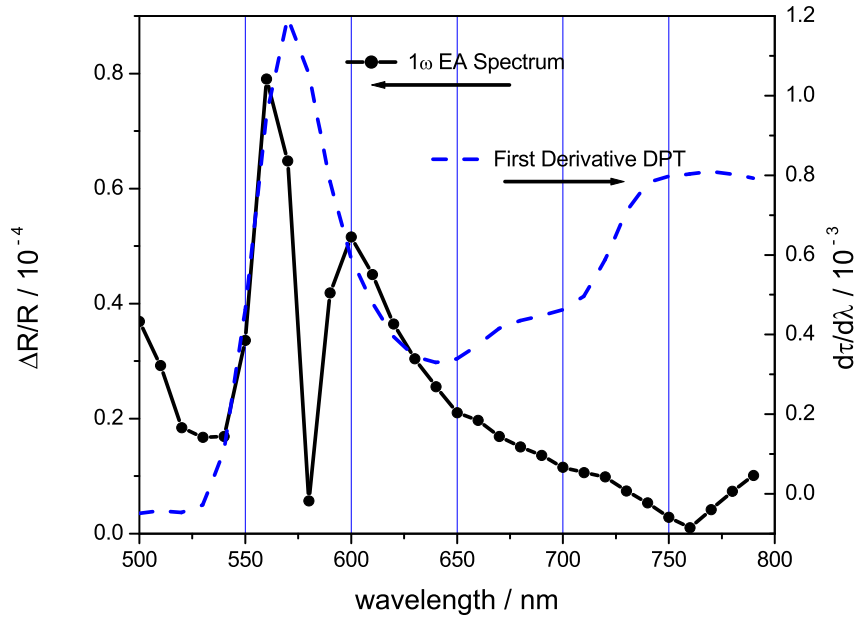


Figure 3.47: 1ω EA spectrum of an ITO - PEDOT - MDMO-PPV/PCBM (1:4 in toluene) - LiF - Al device measured at room temperature compared with the first derivative of the double path transmission (DPT) spectrum; -2 V offset, 2 V amplitude.

ing besides the peak at 570 nm which both spectra have in common one at 610 nm and a broad one peaking around 840 nm.

The largest 1ω EA response is observed at 560 nm, but the signal to noise ratio makes it still almost impossible to determine the internal electric field. As shown in Fig. 3.48, the 1ω EA response in reverse direction can be fitted linearly, but the lines obtained for 1 V respectively 2 V AC amplitude do not intersect the zero line at the same voltage.

Going down with the temperature to 77 K lowers the noise level. At 77 K the agreement between the 1ω EA spectrum and the first derivative of the double path transmission spectrum is better than at room temperature (Fig. 3.50).

The attempt to determine the internal electric field using the 1ω EA signal at 580 nm shown in Fig. 3.51 allows to find a minimum for the EA response at approximately 0.4 V. Fitting the 1ω EA at different AC amplitudes does not lead to the same point of intersection with the zero line. This is observed in the data collected at room temperature (Fig. 3.48) as well as at 77 K (Fig. 3.51). The 1ω EA spectrum shows two other peaks, at which

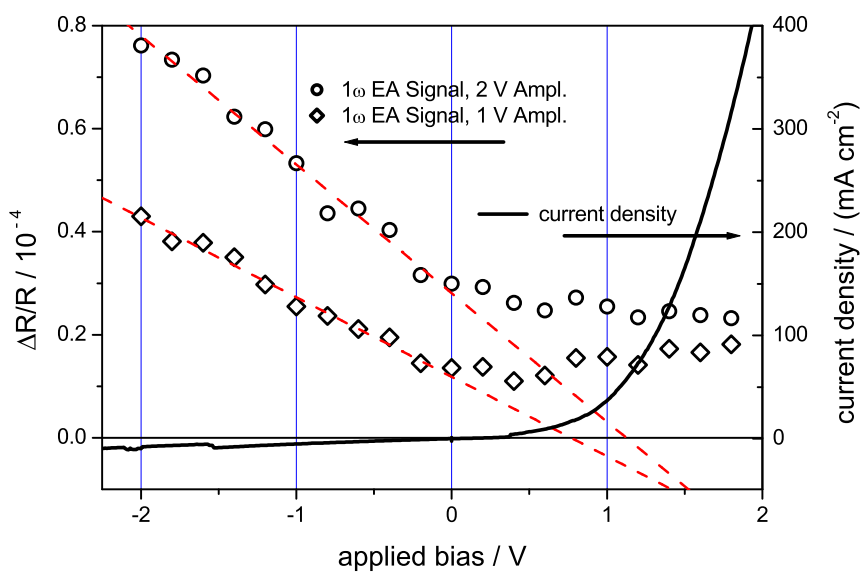


Figure 3.48: Internal electric field measurement and the J-V curve of an ITO - PEDOT - MDMO-PPV/PCBM (1:4 in toluene) - LiF - Al device at room temperature probed at 560 nm; 2 V amplitude (circles) and 1 V amplitude (diamonds).

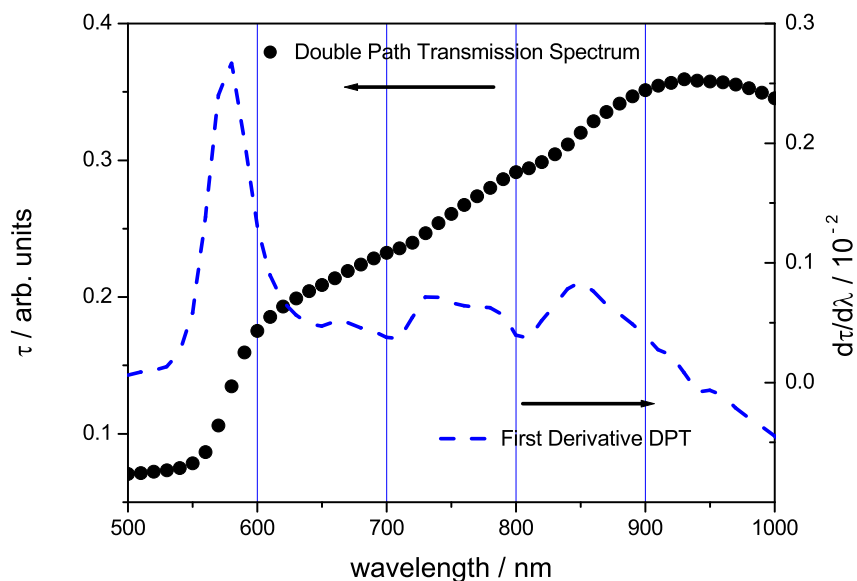


Figure 3.49: Double path transmission (DTP) spectrum of an ITO - PEDOT - MDMO-PPV/PCBM (1:4 in toluene) - LiF - Al device measured at 77 K and its first derivative.

the voltage dependence of the EA signal can be measured.

In Fig. 3.52 and Fig. 3.53, the results of these experiments are presented. Though relatively noisy, the results show good consistency and show a significant change of the phase of the lock-in signal. In Fig. 3.52, the linear fits of the EA signals in reverse direction both intersect the zero line at approximately the same value: 0.5 V.

Probing at 840 nm even allows to observe the characteristic V-shape of the 1ω EA signal. The minimum is at approximately 0.5 V.

Due to the increased film roughness being a morphology effect, the reflection on the Al electrode is diffuse in the case of MDMO-PPV/PCBM films spun from toluene. Therefore EA studies done in reflection geometry (double path transmission, see section 2.1) cannot provide low noise level results.

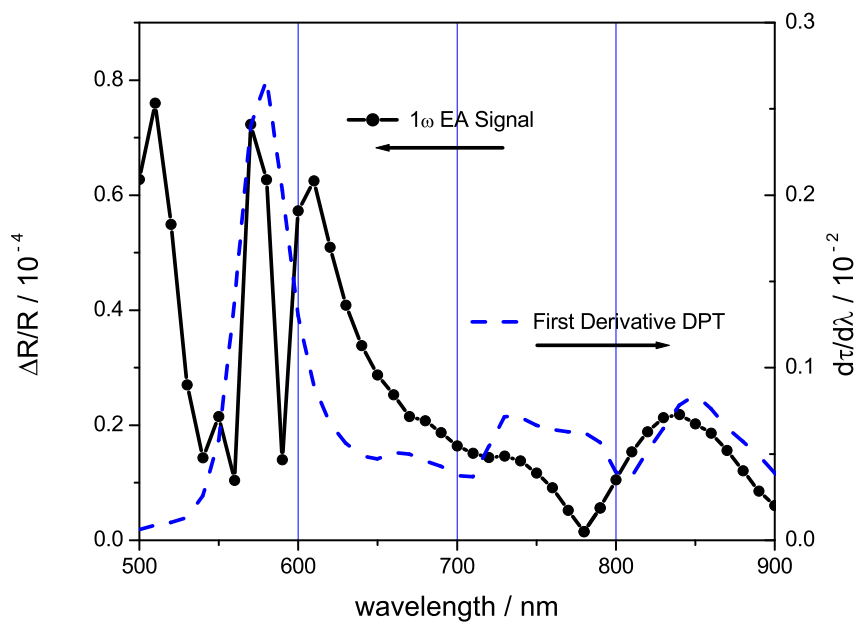


Figure 3.50: 1ω EA spectrum of an ITO - PEDOT - MDMO-PPV/PCBM (1:4 in toluene) - LiF - Al device measured at 77 K compared to the first derivative of the double path (DTP) transmission spectrum; -2 V offset, 2 V amplitude.

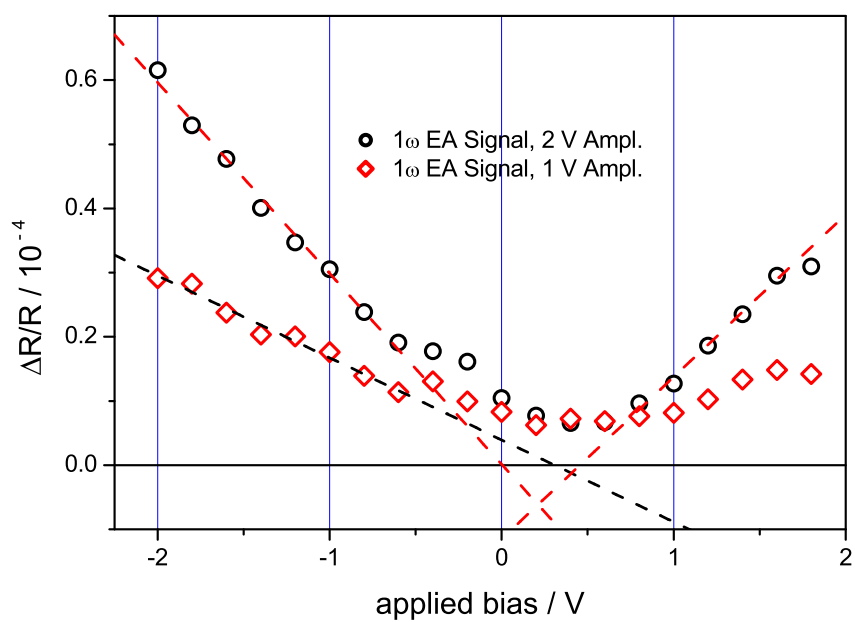


Figure 3.51: Internal electric field measurement of an ITO - PEDOT - MDMO-PPV/PCBM (1:4 in toluene) - LiF - Al device at 77 K probed at 580 nm; 2 V amplitude (circles) and 1 V amplitude (diamonds).

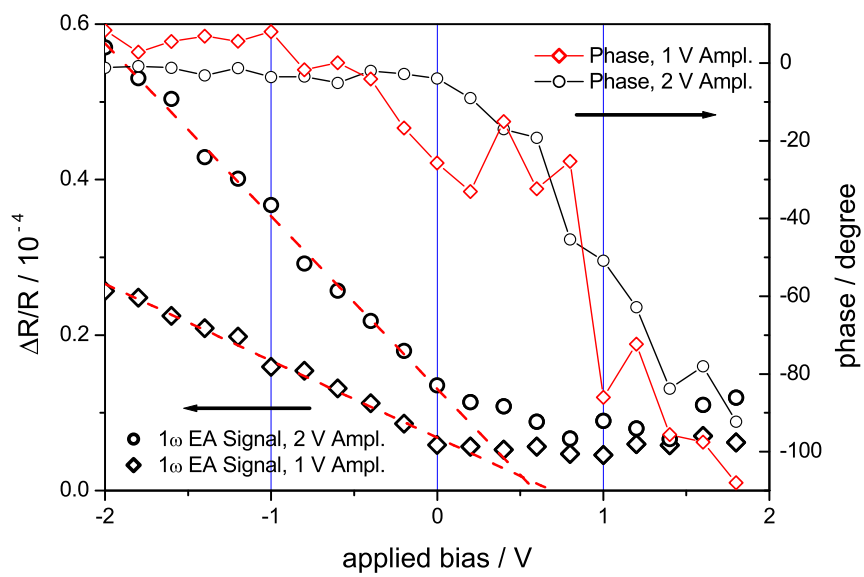


Figure 3.52: Internal electric field measurement of an ITO - PEDOT - MDMO-PPV/PCBM (1:4 in toluene) - LiF - Al device at 77 K probed at 610 nm; 2 V amplitude (circles) and 1 V amplitude (diamonds).

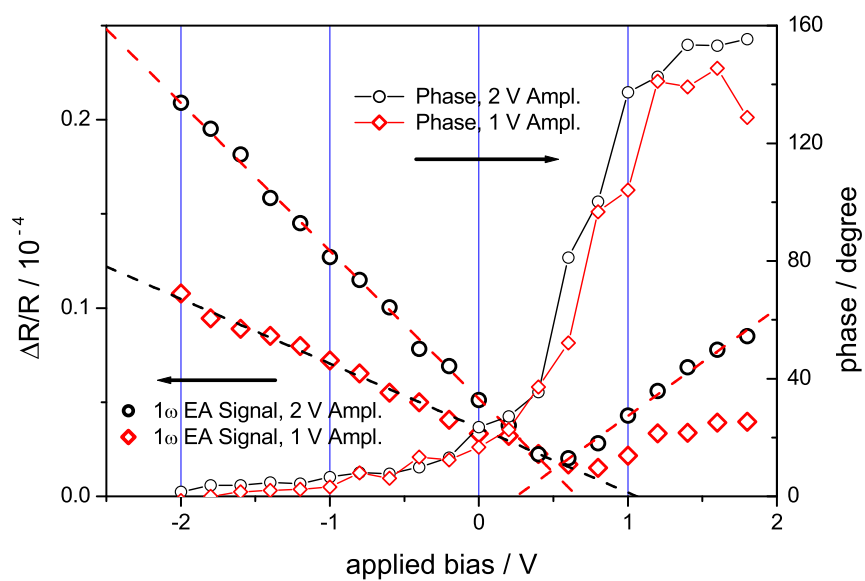


Figure 3.53: Internal electric field measurement of an ITO - PEDOT - MDMO-PPV/PCBM (1:4 in toluene) - LiF - Al device at 77 K probed at 840 nm; 2 V amplitude (circles) and 1 V amplitude (diamonds).

3.5 P3HT/PCBM Blends

3.5.1 Untreated Devices Employing P3HT/PCBM Blends as Active Layer

The active layers are spin cast onto PEDOT:PSS coated ITO on glass substrates and are made of P3HT/PCBM blends (1:2) in chloroform. For details on the production process see section 2.2 on page 14.

The samples from which the results of this section are obtained do not undergo any special treatment prior to the installation into the cryostat inside the glove box. Just as the MDMO-PPV/PCBM blends before, the dou-

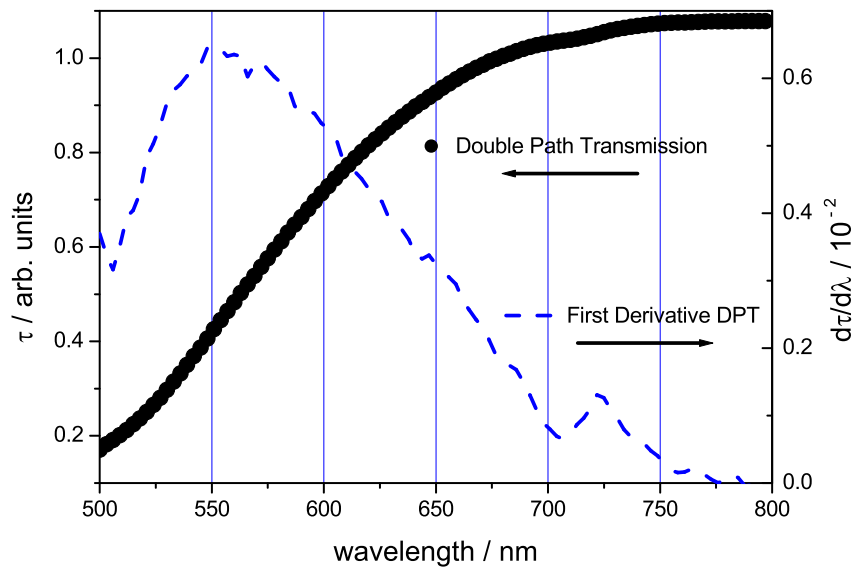


Figure 3.54: Double path transmission spectrum of an untreated ITO - PEDOT - P3HT/PCBM (≈ 100 nm, 1:2 in chloroform) - LiF - Al device at room temperature and its first derivative.

ble path transmission spectrum of the untreated P3HT/PCBM (Fig. 3.54) closely resembles the spectrum of pure PCBM (Fig. 3.36). From the first derivative a broad EA peak around 550 nm is expected. The 1ω EA spectrum shown in Fig. 3.55 shows only poor agreement with the first derivative of the double path transmission spectrum. Only one distinct peak around 540 nm is observed, the rest of spectrum remains featureless.

Going from DC offsets of -2 V to -1 V and then 0 V, the EA response decreases. At 1 V and 2 V in forward direction, no EA signal can be observed at all. The large injection current screens the applied electric field.

At wavelengths below 550 nm the absorption of the sample is very high and

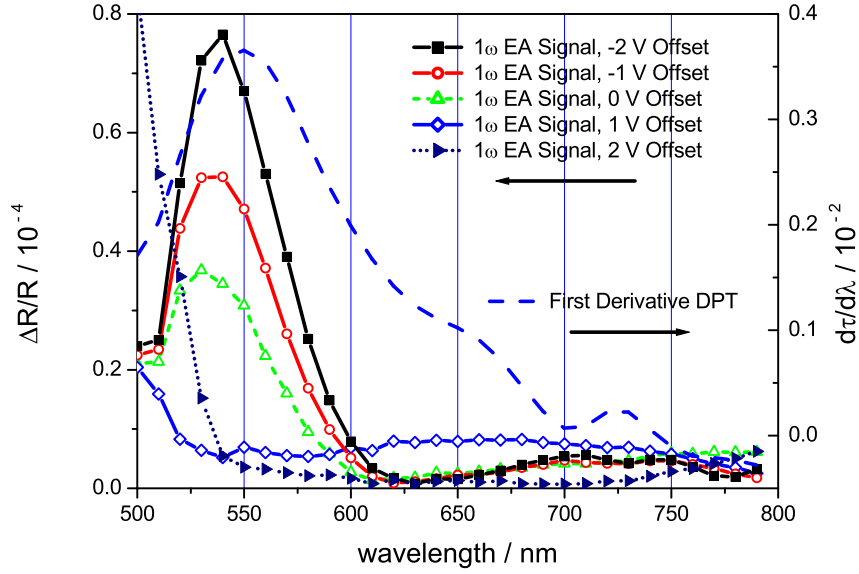


Figure 3.55: 1ω EA spectra measured with DC offsets varying from -2 V to 2 V, 1 V amplitude of an untreated ITO - PEDOT - P3HT/PCBM (≈ 100 nm, 1:2 in chloroform) - LiF - Al device at room temperature compared with the first derivative of the double path transmission (DPT) spectrum.

at the same time the light intensity delivered by the lamp is weak (compare Fig. 2.3). At 2 V offset basically no EA response is measured, therefore for the normalization $\Delta R/R$ two very small signals are divided, pretending a signal between 500 nm and 550 nm.

The internal electric field at room temperature is determined using the 1ω EA signal at 550 nm (Fig. 3.56). In reverse direction the measured points can be fitted with a straight line. Extrapolating these lines, the point of intersection with the zero line is 2.1 V. But exactly where the DC offset plus the AC amplitude overshoots the threshold voltage of beginning charge injection, the EA response decreases and reaches zero at 1 V, the turn-on voltage.

In Fig. 3.56 this point of abruptly changing slopes is located between 0.4 V and 0.6 V for 1 V peak-to-peak AC amplitude (circles) and between 0.6 V and 0.8 V for 0.5 V AC amplitude (diamonds).

Fig. 3.57 shows the 1ω EA spectrum at 77 K of the untreated ITO - PEDOT - P3HT/PCBM (1:2) - LiF - Al device. The dependence of the EA spectra on the applied DC bias at 77 K is very similar to the behavior at room temperature (Fig. 3.55). Though the J-V curve at 77 K is symmetric around zero and the current density is low, if forward bias is applied, the

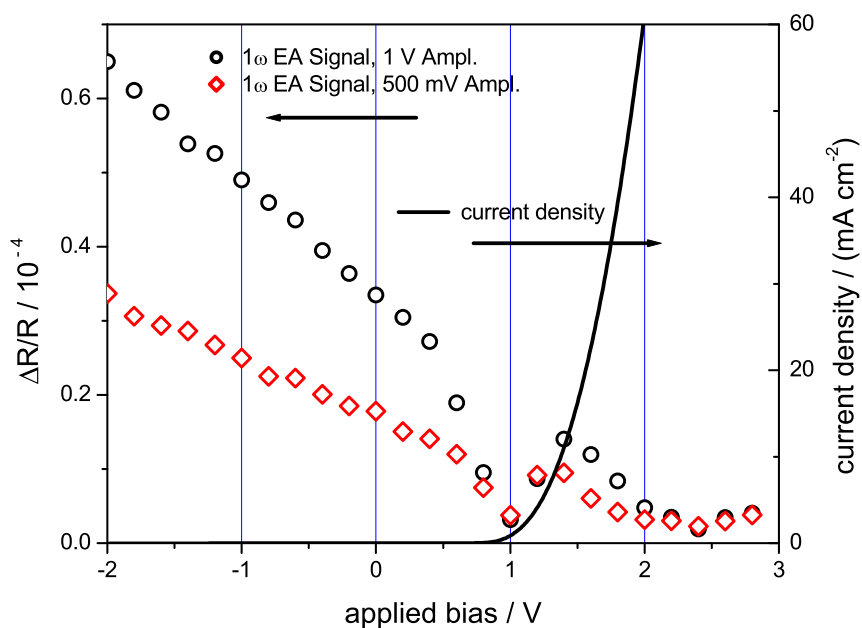


Figure 3.56: Internal electric field measurement and J-V curve of an untreated ITO - PEDOT - P3HT/PCBM (≈ 100 nm, 1:2 in chloroform) - LiF - Al device at room temperature probed at 550 nm; 1 V and 500 mV amplitude.

EA is smaller than in reverse direction. The reason for this is, that over 1 V have to be applied to overcome the internal electric field. Unlike in the experiment at room temperature, at applied forward bias the EA response at 550 nm is small, but remains visible.

The determination of the internal electric field at 77 K shows a different result than at room temperature. In Fig. 3.58 the EA response to a variation of the DC offset can be fitted linearly. The fits of the falling and the rising branch intersect the zero line at 1.4 V.

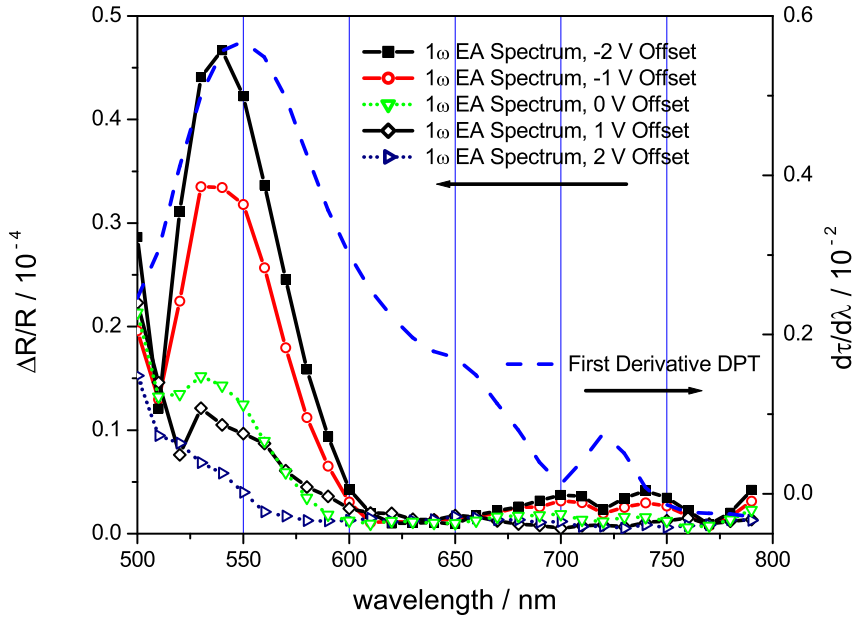


Figure 3.57: 1ω EA spectra measured with DC offsets varying from -2 V to 2 V , 1 V amplitude of an untreated ITO - PEDOT - P3HT/PCBM (≈ 100 nm, 1:2 in chloroform) - LiF - Al device at 77 K compared with the first derivative of the double path transmission (DPT) spectrum.

3.5.2 P3HT/PCBM Blends after Postproduction Treatment

Samples of the structure ITO - PEDOT -P3HT/PCBM (2:3) - LiF - Al were prepared by spin-casting the active layer from a solution in chloroform. After evaporating the reflecting back electrode, the devices underwent the so-called postproduction treatment, a combined heat and electric refining step of the active layer. General information about the postproduction treatment were published by Franz Padinger et al. and can be found in reference [25]. For details on the actual treatment conditions of these samples see section 2.2 on page 14.

As the double path transmission spectrum in Fig. 3.59 shows, the post-production treatment has an indisputable impact on the absorption of the P3HT/PCBM film. Now the absorption reaches to longer wavelengths. Even with the naked eye the change of the color from a brownish yellow to deep purple can be observed.

The first derivative of the double path transmission spectrum shows peaks at 570 nm and 630 nm, in the untreated films there was only a broad feature peaking around 550 nm (Fig. 3.54). In the 1ω EA spectrum (Fig. 3.60)

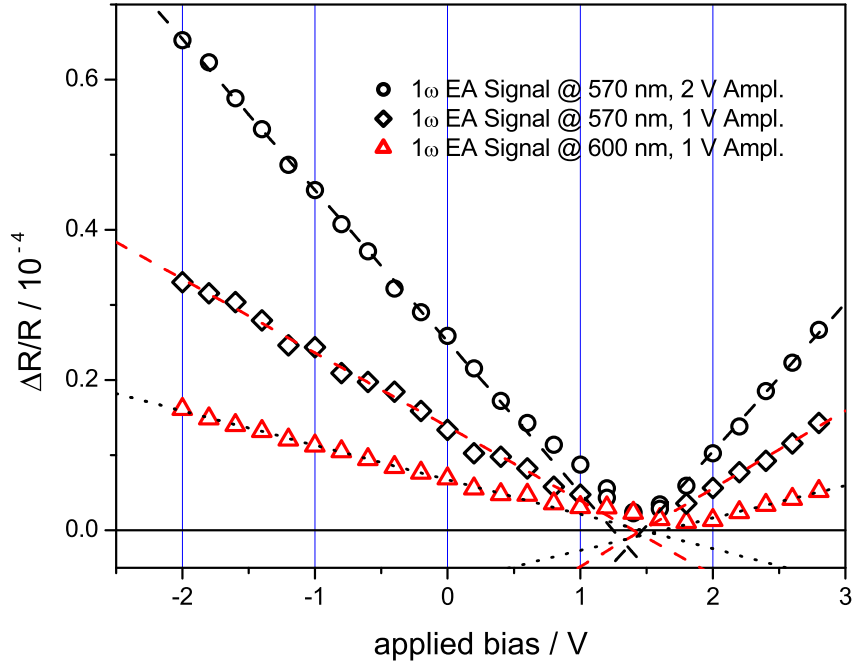


Figure 3.58: Internal electric field measurement of an untreated ITO - PE-DOT - P3HT/PCBM (≈ 100 nm, 1:2 in chloroform) - LiF - Al device at 77 K probed at 570 nm (1 V and 2 V amplitude) and 600 nm (1 V amplitude).

at applied reverse bias the line shape up to 650 nm coincides with the first derivative of the double path transmission spectrum: the peaks at 570 nm and 630 nm are present in both spectra.

From 650 nm on another broad peak is present in the 1ω EA spectrum reaching its maximum at 700 nm which is not expected from the transmission spectrum.

Fig. 3.60 also shows that the spectral EA response of the treated devices is heavily influenced by the applied DC offset. In reverse direction, reducing the offset from -2 V to -1 V diminishes the EA at the first two peaks at 570 nm and 630 nm but leaves the third at 700 nm unaffected. Modulating around 0 V, the formerly dominating peaks at 570 nm and 630 nm have almost vanished, while the response at 700 nm is increased. When the device is biased with 0.8 V, the voltage at which Fig. 3.61 shows the highest response to the bias, the whole spectrum changes:

Around 610 nm, a new peak arises between the two peaks of the first derivative of the double path transmission spectrum and the peak around 700 nm increases dramatically. Fig. 3.61 shows the attempt to determine the inter-

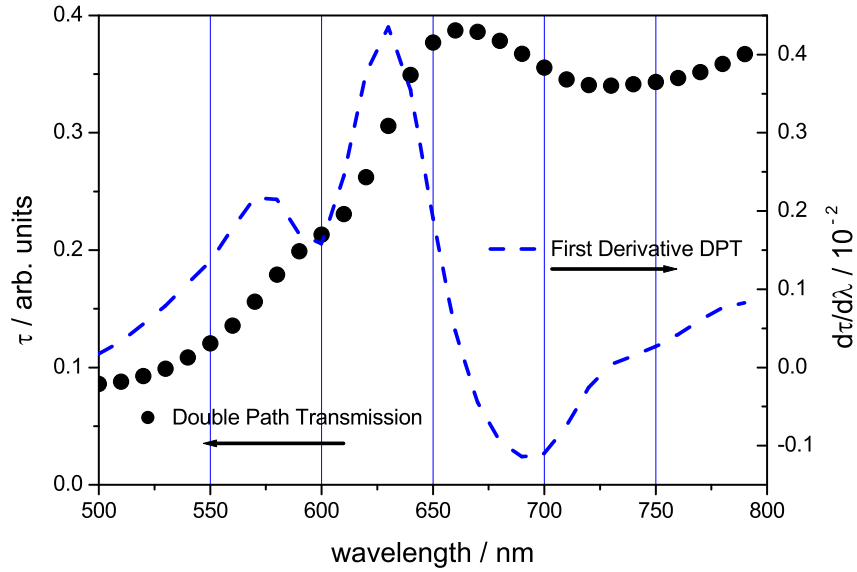


Figure 3.59: Double path transmission (DPT) spectrum of a treated ITO - PEDOT - P3HT/PCBM (≈ 150 nm, 2:3 in chloroform) - LiF - Al device at room temperature and its first derivative.

nal electric field of an ITO - PEDOT - P3HT/PCBM (2:3 in chloroform) - LiF - Al device at room temperature. The EA response does not follow a straight line and once DC offset plus AC amplitude exceed the turn-on voltage the signal increases, peaks at the turn-on voltage of 0.8 V and decreases again obscuring the EA and making it impossible to determine the internal electric field.

In Fig. 3.61 it is clearly seen, that by decreasing the AC amplitude the onset of the obscuring peak is shifted more closely to the turn-on voltage.

The 1ω EA spectrum at 77 K is shown in Fig. 3.62. The results obtained with negative applied voltages show the same behavior as at room temperature: Peaks at 580 nm, 640 nm and 700 nm are observed. In forward direction the third peak at 700 nm dominates the spectrum.

At 77 K no obscuring peak disturbs the attempt to determine the internal electric field (Fig. 3.63). Though the 1ω EA signal does not follow a straight line, the signal vanishes at 1 V to increase again with higher DC offsets.

The internal electric field that has to be overcome to cancel the Stark effect is equal to 1 V.

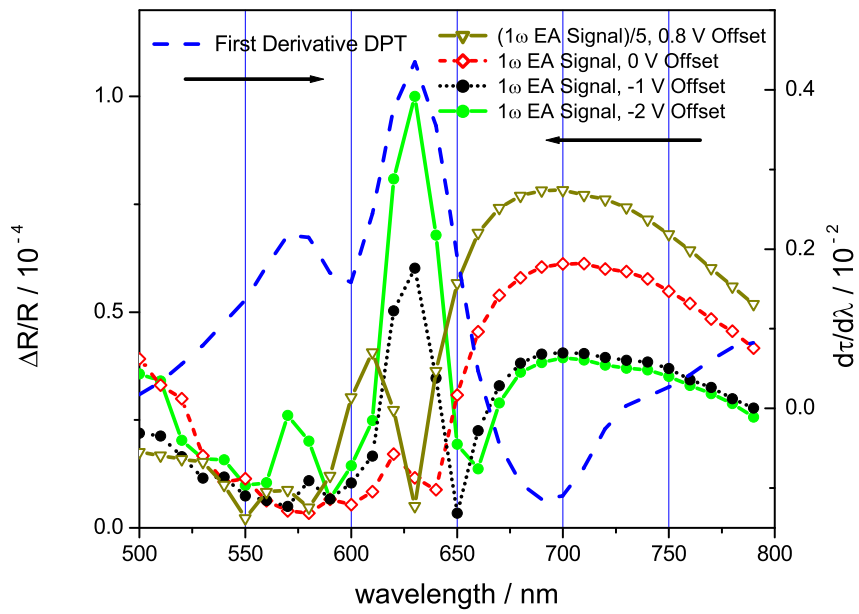


Figure 3.60: 1ω EA spectra measured with DC offsets varying from -2 V to 0.8 V of a treated ITO - PEDOT - P3HT/PCBM (≈ 150 nm, 2:3 in chloroform) - LiF - Al device at room temperature compared with the first derivative of the double path transmission (DPT) spectrum; 1 V amplitude. The EA spectrum at 0.8 V DC is divided by 5.

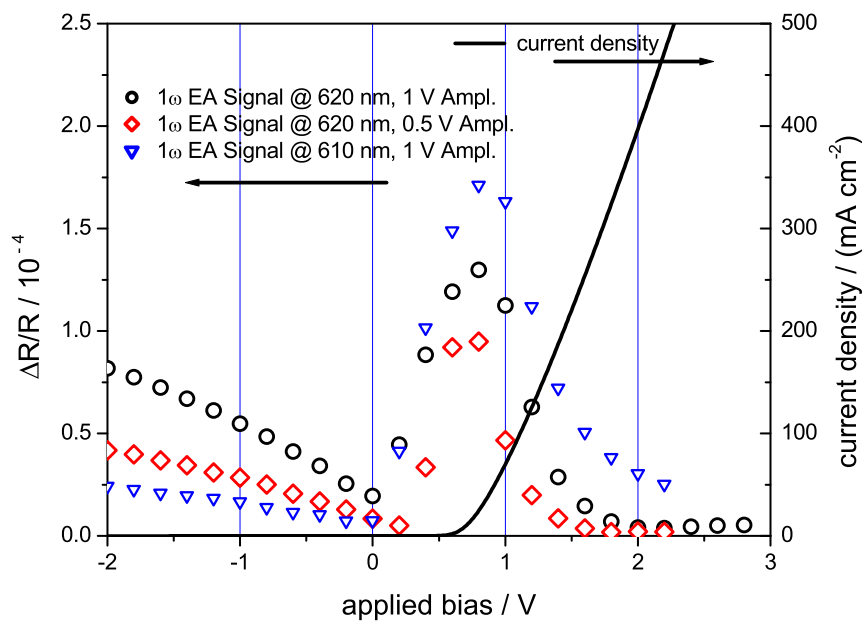


Figure 3.61: Internal electric field measurement and the J-V curve of a treated ITO - PEDOT - P3HT/PCBM (≈ 150 nm, 2:3 in chloroform) - LiF - Al device at room temperature probed at 610 nm and 620 nm.

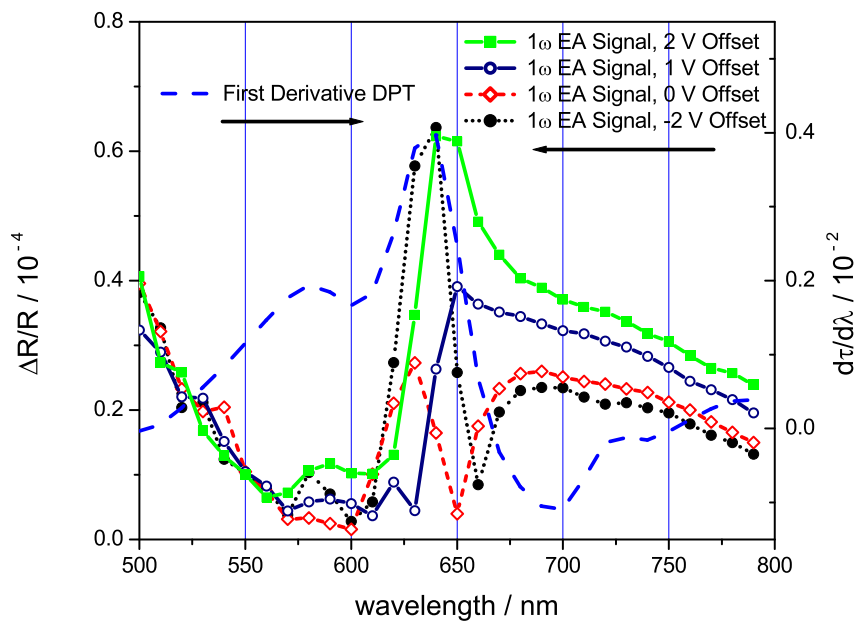


Figure 3.62: 1ω EA spectra measured with DC offsets varying from -2 V to 2 V of a treated ITO - PEDOT - P3HT/PCBM (≈ 150 nm, 2:3 in chloroform) - LiF - Al device at 77 K (1 V amplitude) compared with the first derivative of the double path transmission (DPT) spectrum.

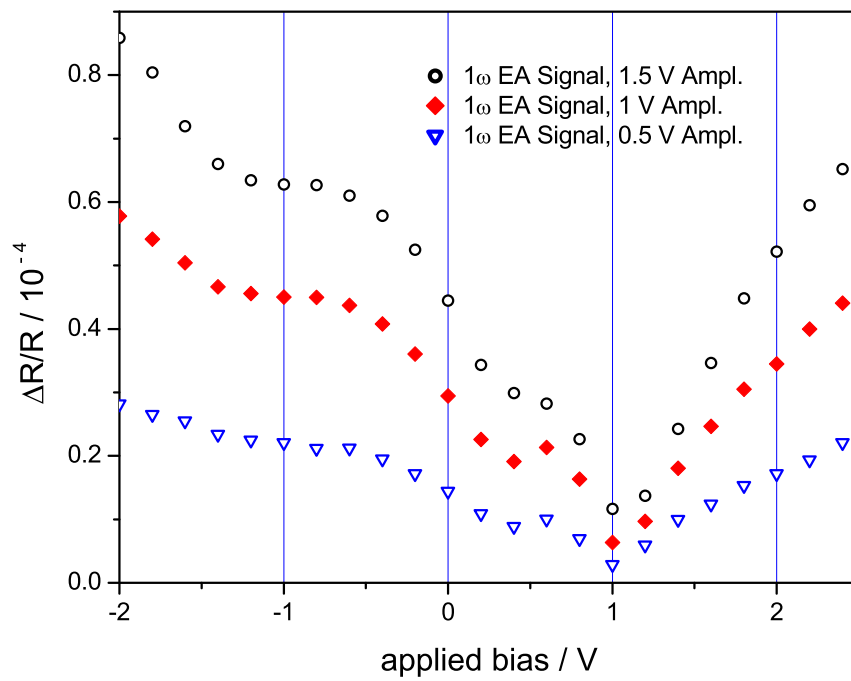


Figure 3.63: Internal electric field measurement of a treated ITO - PEDOT - P3HT/PCBM (≈ 150 nm, 2:3 in chloroform) - LiF - Al device at 77 K probed at 630 nm; 0.5 V (triangles), 1 V (diamonds) and 1.5 V amplitude (circles).

Chapter 4

Conclusion

As long as perturbing effects like major charge carrier injection are ruled out, the results presented in chapter 3 generally show good agreement with the mathematical treatment introduced in chapter 1: If operated below the turn-on voltage or at 77 K, the EA spectra presented above coincide with the corresponding first derivatives of the DPT spectra. Following the argumentation in reference [11], the energy gap between the ground state and the first excited state exhibits the dominant $1B_u$ Stark shift [23] resulting in the first derivative line shape.

Only for the devices employing a layer of pristine PCBM (Fig. 3.39), the agreement has to be considered as poor. But also this fact does not contradict the findings in section 1.3.2, because unlike in the luminescent polymers in fullerenes the ground state and the first excited state are of the same parity [28] making this transition not allowed.

In injection regime also deviations from the first derivative line shape have been observed, most prominent for devices with an active layer made of post-treated P3HT/PCBM (Fig. 3.60). Effects due to the current flow superimposing the EA response have been frequently reported in the literature and were identified as: electric field screening [29], absorption bleaching [31] excited state absorption of trapped charge [29].

Also the linearity between 1ω EA signal and DC offset, which is directly based on the dependence of the EA on the square of the electric field (see equation (1.12) in section 1.3.2) holds in reverse direction or at 77 K.

The devices employing pristine P3HT and P3HT/PCBM blends are the exception: The linearity hardly holds at all, indicating a connection with the material properties of P3HT.

The non linear behavior of the J-V curves indicates space charge limited current [32] transport in the devices resulting in a highly inhomogeneous electric field across the active layer. This violates the condition of a spa-

tially homogeneous electric field being a fundamental assumption for the theoretical approach leading to equation ((1.12) in section 1.3.2).

While in many papers on EA [17, 18, 19, 20, 26], the authors aim to find the device's built-in potential, defined as the difference in the work functions of anode and cathode, this was not the goal of this work. The experiments presented above should characterize state of the art PLEDs and bulk heterojunction solar cell devices and identify the effects of interfacial layers on the internal electric field present in the materials used for these devices. Following the idea of I. Parker [33], who described PLEDs below the turn-on voltage as a metal/insulator/metal combination (MIM picture), the internal electric field should be equal to the difference in the work functions of the contact materials as long as their Fermi levels are located within the HOMO and the LUMO levels of the conjugated polymer sandwiched between the contacts.

To my understanding, one has to be careful to apply this picture to the results presented above.

ITO does not possess a well defined work function, though in literature a value of around 4.7 eV is widely used. It is known, that the work function of ITO is sensitive to the fabrication process [34] as well as to preparation conditions [35].

Taking ≈ 4.7 eV for the ITO work function, ≈ 5.0 eV for PEDOT:PSS and 4.3 eV for Al, the model can neither explain the experimentally determined values nor the difference in the internal electric field between MDMO-PPV and P3HT.

I. Parker explicitly based his model on depleted films, which therefore cannot account for space charge in the contact region, that was reported to be present and to influence EA measurements in sandwich device geometry [11]. Any charge accumulation would influence the internal electric field. Nonlinearities in the EA response have already been attributed to charge accumulation at interfaces in the literature [36]. Furthermore Parker's model does not explain the observed differences of room temperature and 77 K experiments.

The direction of the internal electric field is the same in all devices presented above: A certain external forward bias has to be applied in order to cancel the internal field. Fig. 4.1 presents a possible origin of this internal field due to accumulation of positive charges on the interface between active layer and cathode and negative charges on the anodic side. Injecting electrons via the Al and holes via the ITO causes recombination and therefore the electric field vanishes.

The influence of interfacial layers on the internal field would then be related to a modification of the injection barrier and therefore to the charge carrier injection properties. Lowering the temperature has a significant impact on

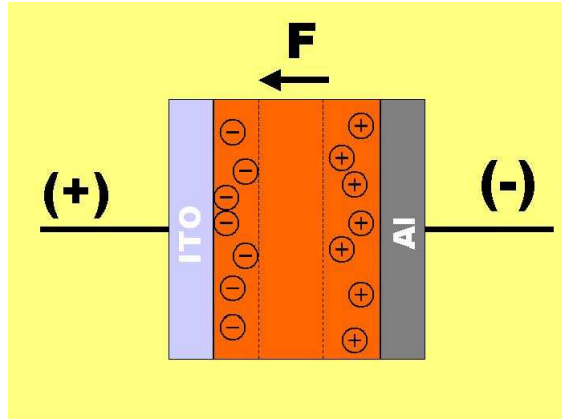


Figure 4.1: Charging up the contact region of the active layer leads to an internal electric field needing an external forward bias to cancel it.

the mobility. At 77 K the charge carriers in the conducting polymers are almost immobile. This will hamper their movement through the layer and prevent recombination and would be a possible explanation for the fact, that the internal electric field is always higher at low temperature than at room temperature.

EA studies on polymer/fullerene bulk heterojunction photovoltaic devices have been reported by Heller et al. [18]. They observed a reduction of the internal electric field measured at room temperature in devices with C_{60} doped MEH-PPV active layers compared to the pristine polymer [18]. The conclusion of that paper is, that the C_{60} doping of the polymer layer introduces an electron acceptor level into the band gap of the polymer below the work function of the cathode. This additional states will lead to charge transfer between the contact and the C_{60} resulting in chemical potential pinning.

In this work the results of EA studies on bulk heterojunction solar cells are presented in section 3.4 and 3.5. At room temperature approximately 1 V was found to be sufficient to cancel the internal electric field in MDMO-PPV/PCBM devices spin cast from a solution in chlorobenzene (Fig. 3.44) and P3HT/PCBM devices (Fig. 3.56 and Fig. 3.61). This bias equals the internal field found for ITO - PEDOT - PCBM - LiF - Al devices.

These findings confirm the experimental results in [18], but not necessarily the interpretation presented in that paper, because experiments at 77 K resulted in different values for the internal electric field (Fig. 3.45, Fig. 3.58 and Fig. 3.62).

Bibliography

- [1] H. Shirakawa, E.J. Louis, A.G. MacDiarmid, C.K. Chiang, and A.J. Heeger. *J. Chem. Soc. Chem. Comm.*, 16:578 – 580, 1977.
- [2] C.K. Chiang, C.R. Fincher Jr, Y.W. Park, A.J. Heeger, E.J. Louis H. Shirakawa, S.C. Gau, and A.G. MacDiarmid. *Phys. Rev. Lett.*, 39(17):1098 – 1101, 1977.
- [3] C.K. Chiang, M.A. Druy, S.C. Gau, A.J. Heeger, E.J. Louis, A.G. MacDiarmid, Y.W. Park, and H. Shirakawa. *J. Am. Chem. Soc.*, 100:1013, 1978.
- [4] U. Wolf, S. Bart, and H. Bässler. *Appl. Phys. Lett.*, 75:2035 – 2037, 1999.
- [5] J.C. deMello, J.J.M. Halls, S.C. Graham, N. Tessler, and R.H. Friend. *Phys. Rev. Lett.*, 85:421 – 424, 2000.
- [6] P.W.M. Blom, M.J.M. de Jong, and C.T.H.F. Lidenbaum. *Poly. Adv. Techn.*, 9:390 – 401, 1998.
- [7] A.J. Campbell, M.S. Weaver, D.G. Lidzey, and D.D.C. Bradley. *J. Appl. Phys.*, 84:6737 – 6739, 1998.
- [8] I.H. Campbell, D.L. Smith, C.J. Neef, and J.P. Ferraris. *Appl. Phys. Lett.*, 75:841 – 843, 1999.
- [9] C. Giebeler, S.A. Whitelegg, D.G. Lidzey, P.A. Lane, and D.D.C. Bradley. *Appl. Phys. Lett.*, 75:2144, 1999.
- [10] F. Rohlfig, T. Yamada, and T. Tsutsui. *J. Appl. Phys.*, 86:4978 – 4984, 1999.
- [11] G. Weiser and A. Horvath. *Primary photoexcitations in conjugated polymers: Molecular exciton versus semiconductor band model*, chapter 12, Electroabsorption spectroscopy on π -conjugated polymers. Edited by N.S. Sariciftci, World Scientific, Singapore, 1997.
- [12] D.E. Aspnes and A. Frova. *Solid State Comm.*, 7:155 – 159, 1969.

- [13] D.E. Aspnes and J.E. Rowe. *Phys. Rev. B*, 5(10):4022 – 4030, 1972.
- [14] S.D. Phillips, G. Yu, T. Hagler, R. Freedman, Y. Cao, V. Yoon, J. Chiang, W.C. Walker, and A.J. Heeger. *Phys. Rev. B*, 40(14):9751 – 9759, 1989.
- [15] A. Horvath, G. Weiser, G.L. Baker, and S. Etemad. *Phys. Rev. B*, 51(5):2751 – 2758, 1995.
- [16] G. Weiser and A. Horvath. *Chem. Phys.*, 227:153 – 166, 1998.
- [17] I.H. Campbell, T.W. Hagler, D.L. Smith, and J.P. Ferraris. *Phys. Rev. Lett.*, 76:1900 – 1903, 1996.
- [18] C.M. Heller, I.H. Campbell, D.L. Smith, N.N. Barashkov, and J.P. Ferraris. *J. Appl. Phys.*, 81(7):3227 – 3231, 1997.
- [19] T.M. Brown, J.S. Kim, R.H. Friend, F. Cacialli, R. Daik, and W.J. Feast. *Appl. Phys. Lett.*, 75(12):1679 – 1681, 1999.
- [20] T.M. Brown, R.H. Friend, I.S. Millard, D.L. Lacey, J.H. Burroughes, and F. Cacialli. *Appl. Phys. Lett.*, 77(19):3096 – 3098, 2000.
- [21] J. Yoon, J. Kim, T. Lee, and O. Park. *Appl. Phys. Lett.*, 76(16):2152 – 2154, 2000.
- [22] L. Pedrotti and L.S. Pedrotti. *Optik*, chapter 26, Nichtlineare Optik und Lichtmodulation. Prentice Hall, München, 1996.
- [23] M. Liess, S. Jeglinsky, Z. V. Vardeny, M. Ozaki, K. Yoshino, Y. Ding, and T. Barton. *Phys. Rev. B*, 56(24):15712 – 15724, 1997.
- [24] F. Feller and A.P. Monkman. *Phys. Rev. B*, 60(11):8111 – 8116, 1999.
- [25] F. Padinger, R. Rittberger, and N.S. Sariciftci. *Adv. Funct. Mater.*, 13(2):1–4, 2003.
- [26] T.M. Brown, R.H. Friend, I.S. Millard, D.L. Lacey, T. Butler, J.H. Burroughes, and F. Cacialli. *J. Appl. Phys.*, 93(10):6159 – 6172, 2003.
- [27] B.A. Mattis, P.C. Chang, and V. Subramanian. *Mat. Res. Soc. Symp. Proc.*, 771, 2003.
- [28] M.S. Dresselhaus, G. Dresselhaus, and P.C. Eklund. *Science of fullerenes and carbon nanotubes*, chapter 12, Electronic Structure. Academic Press, New York, 1996.
- [29] P.A. Lane, J.C. deMello, R.B. Fletcher, and M. Bernius. *Appl. Phys. Lett.*, 83(17):1 – 3, 2003.

- [30] T. Martens, J. D'Haen, T. Munters, L. Goris, Z. Beelen, J. Manca, M. D'Olieslaeger, D. Vanderzande, L. De Schepper, and R. Andriessen. *Mat. Res. Soc. Symp. Proc.*, 725, 2002.
- [31] I.H. Campbell, D.L. Smith, C.J. Neef, and J.P. Ferraris. *Appl. Phys. Lett.*, 78(3):270 – 272, 2001.
- [32] M.A. Lampert and P. Mark. *Current injection in solids*, chapter 1, One carrier currents. Academic Press, New York, 1970.
- [33] I.D. Parker. *J. Appl. Phys.*, 75(3):1656–1666, 1994.
- [34] J.S. Kim, M. Granström, R.H. Friend, N. Johansson, W.R. Salaneck, R. Daik, W.J. Feast, and F. Cacialli. *J. Appl. Phys.*, 84:6859, 1998.
- [35] P.A. Lane, J. Rostalski, C. Giebeler, S.J. Martin, D.D.C. Bradley, and D. Meissner. *Sol. Energy Mater. Sol. Cells*, 63:3 – 13, 2000.
- [36] I. Hiromitsu, Y. Murakami, and T. Ito. *J. Appl. Phys.*, 94(4):2434 – 2439, 2003.

CURRICULUM VITAE

Christoph Lungenschmied
Leonfeldnerstr. 101 a
4040 Linz, AUSTRIA
Telephone: 0043-650-7312831
E-mail: christoph.lungenschmied@jku.at

Personal Data

Date/Place of Birth: April, 8th 1979 in Linz, Austria
Nationality: Austrian
Marital Status: Unmarried

Education

4/2003 - 4/2004 Diploma Thesis at the Linz Institute for Organic Solar Cells (LIOS)
10/1998 - 7/2004 Johannes Kepler University Linz, Austria
Economics/Chemical Engineering
6/1997 School Leaving Exam passed with Distinction

Military Service

10/1997 - 5/1998 Telecommunication Unit in Linz/Hörsching

Language and Computer Skills

Language : English (fluent), German (mother tongue),
Spanish and French (beginner)
Computer: MS Word, Excel, L^AT_EX, Testpoint, Origin

Special Training and Relevant Occupational Experience

7/ 2002 - 9/2002 Internship at DAINIPPON Ink and Chemicals, Inc. Tokyo, Japan
Analysis Center and Offset Ink Department
4/2002 - 6/2002 Coworker at the Linz Institute for Organic Solar Cells (LIOS)
Project "Excited State Spectroscopy in Organic Photovoltaic Devices"
Summer 2000 Federal Office of Agrobiolgy, Linz
Performing Analysis of Plant Materials

Interests

Travelling, Marathon, Fistball (Upper Austrian Fistball Title 2001/02 and 2003)

List of Publications

- "Electric Field Induced Enhancement of the Photoinduced Absorption in Conjugated Polymer/Fullerene Bulk Heterojunction Solar Cells"
C. Winder, C. Lungenschmied, N.S. Sariciftci, C. Arndt, U. Zhokhavets, G. Gobsch
Submitted to *Organic Electronics*

- "Investigation of Excited States in Polymer/Fullerene Solar Cells by Means of Photoinduced Reflection-/Absorption Spectroscopy"
C. Arndt, U. Zhokhavets, G. Gobsch, C. Winder, C. Lungenschmied, N.S. Sariciftci
Thin Solid Films **451 - 452** (2004), 60 - 63

- "Excited State Spectroscopy in Polymer Fullerene Photovoltaic Devices under Operation Conditions"
C. Winder, C. Lungenschmied, G. Matt, N.S. Sariciftci, A.F. Nogueira, I. Montanari, J.R. Durrant, C. Arndt, U. Zhokhavets, G. Gobsch
Synthetic Metals **139** (2003), 577 - 580

Contributions to Conferences

- "Electroabsorption Studies on Organic Diodes"
C. Lungenschmied, C. Winder, M. Scharber, A. Mozer, G. Matt, H. Neugebauer, N.S. Sariciftci
ICEPOM - 5, 2004 Kiev (Ukraine)

Eidesstattliche Erklärung:

Ich erkläre an Eides statt, dass ich die vorliegende Diplomarbeit selbständig verfasst und keine anderen als die angegebenen Quellen und Hilfsmittel benutzt habe.

Linz, den

.....

(Unterschrift)